

**Geology Underfoot - An Investigation of Jurassic Lacustrine  
Stratigraphy in the Lower Half of the Portland Formation on the  
Campus of Mount Holyoke College**

by

Monica Margarita Geraldés Vega

A Thesis

Presented to the faculty of Mount Holyoke College  
in partial fulfillment of the requirements for the degree of  
Bachelor of Arts with Honors

Department of Geology

Mount Holyoke College

South Hadley, Massachusetts

2022

## **ABSTRACT**

During the summer of 2020, Mount Holyoke College commissioned a geothermal company to drill a 6-inch diameter, 800-foot-deep borehole on campus grounds to measure the geothermal potential of the underlying geology. Professor Al Werner took advantage of this opportunity and collected cuttings during the well drilling operation. These samples were collected every 5 ft and document the detailed stratigraphy of the lower half of Portland formation, a Mesozoic lacustrine shale deposit of the Hartford basin. Geophysical data and imaging provide cm-scale stratigraphic changes and drill cuttings provide samples of the various units. These rocks record environmental conditions during the Early Jurassic. The record is made up of shales and siltstones that alternate in color (red, gray, and dark gray), suggesting changing environmental conditions. This has been confirmed by the existing literature of the Northeast American rift basins. By gathering physical and chemical proxies and finding significant relationships between them and Milankovitch cycles, this study supports previous interpretations that orbital changes explain the borehole stratigraphy. Using these proxies, I describe the changing, lacustrine paleoenvironment of the South Hadley area during the early Jurassic period.

## **TABLE OF CONTENTS**

<b>ABSTRACT</b> .....	<b>2</b>
<b>TABLE OF FIGURES</b> .....	<b>5</b>
<b>TABLE OF TABLES</b> .....	<b>6</b>
<b>ACKNOWLEDGEMENTS</b> .....	<b>7</b>
<b>1 INTRODUCTION</b> .....	<b>9</b>
<b>1.1 A Modern Analogy</b> .....	<b>9</b>
<b>1.2 Rifting in the Connecticut Rift Valley</b> .....	<b>12</b>
<b>1.3 Early Mesozoic Cyclicality</b> .....	<b>13</b>
<b>1.4 Evidence of Lake Level Changes</b> .....	<b>14</b>
<b>1.5 Mount Holyoke College’s 800 ft Borehole</b> .....	<b>15</b>
<b>1.6 Previous Work on Campus</b> .....	<b>17</b>
<b>2 METHODS</b> .....	<b>20</b>
<b>2.1 Field Methods</b> .....	<b>20</b>
<b>2.1.1 Drilling the Well</b> .....	<b>20</b>
<b>2.1.2 Sample collection and processing</b> .....	<b>21</b>
<b>2.1.3 Geophysical Methods</b> .....	<b>23</b>
<b>2.2 Laboratory Methods</b> .....	<b>24</b>
<b>2.2.1 Borehole Cuttings</b> .....	<b>24</b>
<b>2.2.1.1 Color and Appearance</b> .....	<b>25</b>
<b>2.2.2 Magnetic Susceptibility</b> .....	<b>26</b>
<b>2.2.3 Loss on Ignition (LOI)</b> .....	<b>27</b>
<b>2.2.4 X-Ray Fluorescence</b> .....	<b>28</b>
<b>2.2.4.1 Elements used in XRF</b> .....	<b>30</b>
<b>2.2.5 Acycle Software</b> .....	<b>31</b>
<b>2.2.5.1 Sedimentation Rate and Power Spectral Analysis</b> .....	<b>33</b>
<b>2.2.5.2 TimeOpt Analysis</b> .....	<b>35</b>
<b>3 RESULTS</b> .....	<b>37</b>
<b>3.1 Cuttings stratigraphy results</b> .....	<b>37</b>
<b>3.2 OTV Stratigraphy</b> .....	<b>41</b>

3.3 Magnetic Susceptibility .....	44
3.4 Loss on Ignition .....	45
3.5 XRF Results .....	47
3.5.1 Uranium.....	47
3.5.2 Sulfur .....	48
3.5.3. Iron.....	50
3.6 Statistical Analysis based on Natural Gamma ray.....	51
3.6.1 Periodogram/Spectral analysis.....	52
3.6.2 TimeOpt.....	54
4 INTERPRETATIONS.....	56
4.1 Correlation of Cuttings and OTV image.....	56
4.2 Magnetic Susceptibility and Loss on Ignition.....	59
4.3 XRF analyses .....	63
4.3.1 Uranium.....	63
4.3.2. Sulfur& Iron .....	66
4.4 Statistical Interpretation .....	70
4.5 Environmental Interpretation.....	72
5 DISCUSSION .....	78
5.1 Correlation of Well Stratigraphy and Regional Stratigraphy .....	78
5.1 Orbital controls on stratigraphy .....	82
5.2 Open and closed basin conditions .....	83
6 CONCLUSION .....	85
7 FUTURE WORK.....	87
8 REFERENCES.....	89
9 SUPPLEMENTARY MATERIALS .....	94

**TABLE OF FIGURES**

Figure 1.....	11
Figure 2.....	16
Figure 3.....	18
Figure 4.....	24
Figure 5.....	25
Figure 6.....	32
Figure 7.....	34
Figure 8.....	39
Figure 9.....	40
Figure 10.....	42
Figure 11.....	43
Figure 12.....	45
Figure 13.....	46
Figure 14.....	48
Figure 15.....	49
Figure 16.....	50
Figure 17.....	51
Figure 18.....	53
Figure 19.....	55
Figure 20.....	58
Figure 21.....	60
Figure 22.....	62
Figure 23.....	65
Figure 24.....	67
Figure 25.....	68
Figure 26.....	69
Figure 27.....	76
Figure 28.....	80
Figure 29.....	84
Supplementary Figure 1.....	111
Supplementary Figure 2.....	112
Supplementary Figure 3.....	113

**TABLE OF TABLES**

Table 1. MS Raw data.....	94
Table 2. LOI Raw data.....	100
Table 3. XRF Raw data.....	106

## **ACKNOWLEDGEMENTS**

I have so many people to thank for this project. First, my primary advisor, Al Werner: I am eternally grateful for his faith in me and for his exceptional guidance; for sparking my interest in academia and fueling my excitement for geology like no one did during my time at Mount Holyoke; and for constantly supporting me as a student and as an individual. I would like to thank my other two committee members, Amy Nussbaum and Mark McMenam, for helping me discern the more unfamiliar aspects of this research and for the time and effort they put into deciphering the challenging aspects of this project with me. Special thanks go to Dr. Paul Olsen and Clara Chang at Columbia University, whose generosity, time, and graciousness helped me unmask and recognize the significant meaning of this project – their confidence and trust in my work continues to be a big inspiration and drives me to excel in this discipline.

I would like to thank my friends and family for their support during this process – their good humor and love were invaluable during this time. I would specifically like to thank my fellow Geology and Geography thesis students, as their determination helped me keep focus throughout the writing process. I would like to thank my roommate Nayantara Das for entertaining my rambles about geochemistry and paleo-environments. Her passion for learning was a constant reminder that academia is worth pursuing. I would like to thank Raquel Aguirre, who was with me and these rocks since the beginning. And I would also like to thank Rowan Scott, who

was there for me during the great times and the hard times – their support, love, and care was key from start to finish.

Finally, I would like to thank every student, staff, and faculty in the Geology Department of Mount Holyoke College. You all had a part to play in helping me find my passion.

## **1 INTRODUCTION**

Two hundred million years ago, dinosaurs roamed the muddy shorelines of a lake in the Connecticut Rift Valley. The rise of the dinosaurs resulted from the Triassic-Jurassic mass extinction, when extensive volcanism wiped out most vertebrates save for the dinosaurs, allowing them to dominate the Northeast American landscape (Stanley and Luczaj, 2014). The volcanism that helped bring about the mass extinction was caused in part by the rifting of the Atlantic Ocean, which broke up the supercontinent of Pangaea during the Mesozoic. The rifting of the Atlantic Ocean, however, did not happen on the first try - evidence of “stretch marks” are present in the landscape that borders the Atlantic (Little, 2003; Stanley and Luczaj, 2014). Mount Holyoke College and the surrounding area are situated in a failed rift zone (also termed a rift valley or rift basin), called the Connecticut Rift Valley (CRV; Figure 1). Locally, the CRV is called the Hartford rift basin (Kent and Olsen, 2008) and it is bordered by the Eastern border fault which has been inactive for the past 140 million years (Little, 2003).

### *1.1 A Modern Analogy*

A similar active rift zone can be seen in the rift valleys of Eastern Africa (Russell et al, 2020). The African rift valleys present similar climatic conditions to the

Northeast American rift valleys, and similarly contain large deep lakes (e.g., Lake Tanganyika; Figure 1) (Russell et al, 2020). Indeed, the CRV basin, when it was just formed, is thought to have been occupied by a large lake whose depth fluctuated over time – this has been documented in the literature via stratigraphic analysis of other rift valleys, especially the Newark rift basin in New Jersey, New York, and Pennsylvania (Olsen, 1986; Olsen and Kent, 1996, Olsen and Kent, 1999, Olsen et al, 2003, Van Houten, 1962, Baker, 1994).

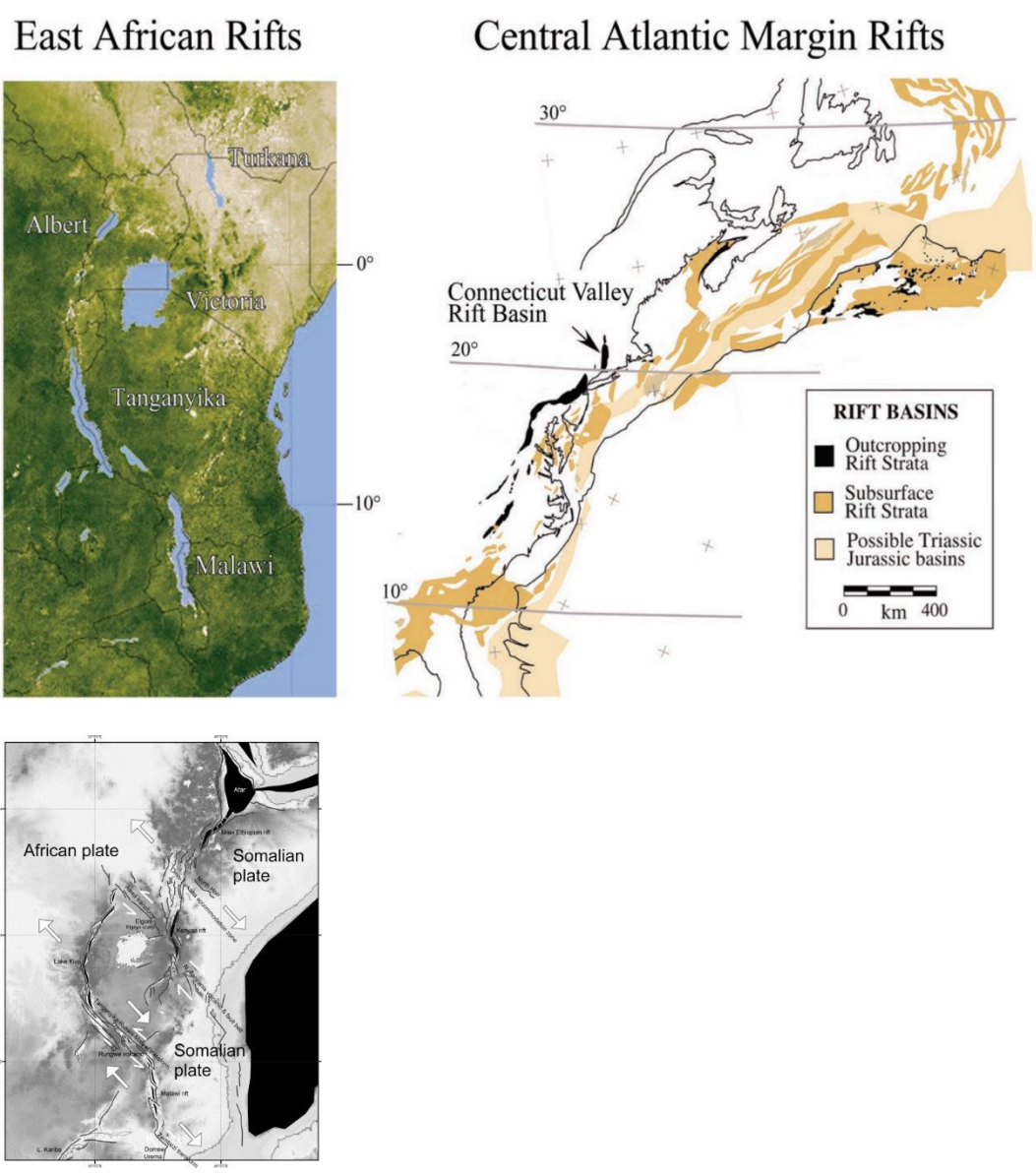


Figure 1. Present East African Rift basins (left) and Northeast American Early Mesozoic rift basins (right). Connecticut Rift Valley (CRV) indicated with black arrow. (from Olsen, 2017). Tectonic elements of the East African Rift basins illustrated in lower left (from Chorowicz, 2005).

### *1.2 Rifting in the Connecticut Rift Valley*

The massive volcanic activity that punctuated the rift valley formation is evidenced by the Central Atlantic Magmatic Province (CAMP), the most wide-spread igneous province in the world composed mostly of basalts spread throughout the East coast of North America and Western Europe and Africa (Olsen, 2017). CAMP records are used extensively as a reference for radiometric dating of stratigraphy below and above these layers, in order to determine the chronology of events during the Mesozoic. Locally, the Holyoke Basalt has been radiometrically dated to be  $201.274 \pm 0.032$  million years in age (Olsen, 2017, Blackburn et al., 2013)

During the Early Jurassic, the Hartford Basin in Connecticut and Massachusetts was located much closer to the equator, at tropical to subtropical latitudes ranging from 12-24°N (Kent and Tauxe, 2005, Whiteside et al., 2011). The proposed local paleoclimate has been described as similar to Central America: humid seasons and dry seasons driven by monsoon strength (Little, 2003). Dinosaurs would have been attracted to the large lake of the Connecticut River Valley and left behind their footprints, as seen on the West side of the Connecticut River in the town of Holyoke (Hitchcock, 1858). Fish and plant fossils are also preserved in the CRV's stratigraphy and suggest a lacustrine setting and environment of deposition (Olsen, 2017). Today, the portion of the CRV in Connecticut and Massachusetts includes sedimentary sequences that record much of the Mesozoic history of Eastern North America (Olsen, 1997).

### *1.3 Early Mesozoic Cyclicality*

Extensive research has elucidated the rifting history of Eastern North America. Chemical and physical variations are present in the stratigraphy of the lacustrine records that indicate changing climatic conditions during the Early Jurassic. In an effort to understand this stratigraphy, rocks in the various rift basins of the Northeast have been studied for over a century. Cyclic sequences derived from visual and chemical changes in the stratigraphy have been identified in the 1960's (Van Houten, 1962). This work has established links between changing lake levels and astronomical forcing in the form of Milankovitch cycles during the Mesozoic for the Newark basin in New Jersey and Pennsylvania (Olsen, 1986, Olsen and Kent, 1996), and for the rest of the CRV. Astronomical forcing has been implicated in long duration and cyclic lake level change during the Jurassic by proposing that changes in the Earth's orbit (eccentricity), axial tilt (obliquity), and axial wobble (precession) undergo periodic changes that are caused by gravitational interactions with other components of the solar system, notably the planets (Schwarzacher, 1993), such as Mars and Jupiter, and the moon, which in turn have their own periodic orbital changes (Laskar et al., 2004). These variations then lead to changes in the amount of insolation that is received by the Earth, thereby impacting the climate. For the tropics of the Jurassic, this would have specifically affected monsoon strength, changes in atmospheric circulation and in turn lake depth (Olsen and Kent, 1996).

As the Milankovitch theory of climate change relies on changing interactions between celestial bodies, projecting back in time under the assumptions that the current periodicities align with periodicities from the Mesozoic is risky because of the recession of the moon and chaos in the solar system (Laskar, 2020). However, existing data based on the North American rift basins suggests that the Milankovitch periods during the Mesozoic were similar to the periods of the present day (Olsen, 1986, Smoot and Olsen, 1994). The sedimentation rate for the Portland formation of the Hartford basin, which is the focus of this study, has been established to be between 0.9 – 1m/1 thousand years (kyr) under the assumption that Milankovitch forcing is driving the changes in lithology (Kent and Olsen, 2008, Sha et al., 2015).

#### *1.4 Evidence of Lake Level Changes*

These lake-level changes are not just theoretical, one is able to “see” these changes in lake depth over time in the local bedrock stratigraphy. Opportunities to study the local bedrock, however, are rare in New England. Outcrops are often limited and infrequent due to an extensive glacial cover. The analysis of continuous stratigraphic sections via boreholes, on the other hand, affords the opportunity to “see” the underlying geology and answer important questions about the geologic past. Specifically, for my study, an 800 ft borehole drilled into the Portland formation is used to reconstruct Jurassic climates and environments. The borehole spans the lower part of the South Hadley Falls member (approx. 0-400 ft) and the upper part of the Park River Member (approx. 400-800 ft) (Olsen, 2003). There is consensus in the

literature about the age of the Portland Formation. Olsen (2003) dated it to be around 1.2 million years younger than the Triassic-Jurassic boundary, placing it in the Lower Jurassic (Hettangian age). This age is determined by basalt (U-Pb) dating from the Central Magmatic Igneous Province (CAMP) that occurs in the section below the Portland Formation, specifically the Holyoke and Hamden basalts and the Talcott Formation (Olsen, 2017). The lacustrine nature of this study's stratigraphic record is particularly interesting as lakes have a relatively simple response to climate (Olsen, 1986). Other paleotropical records in the literature are partly or entirely made up of marine strata, which can become obfuscated by various phenomena, such as polar ice sheets and bioturbation (Olsen and Kent, 1996, Crowley, 1992, Kutzbach and Street-Perrot, 1985). Lacustrine records, on the other hand, have a relatively simple response to climate change, as lake level and salinity (especially in closed basin lakes) have a direct relationship with precipitation and cloud cover, which are determined by climate (Cohen, 2003).

### *1.5 Mount Holyoke College's 800 ft Borehole*

Although the 800 ft borehole drilled on the Mount Holyoke College campus was not drilled for geological purposes, the observable changes in the color of the underlying lacustrine stratigraphy are vivid. This drilling project, contracted by Mount Holyoke College to explore geothermal heating potential of the bedrock, was done near the edge of the campus' rugby field (Figure 2). The project yielded geophysical data and physical cutting samples that were collected during the drilling

of the borehole. Professor Alan Werner and Dr. Jenica Allen saw this as an opportunity to closely examine a stratigraphic record of the underlying geology at the college, and personally collected and organized the drill cuttings at 5 ft intervals. In addition to the 5 ft samples, the Skillings and Sons drilling company lowered geophysical logging equipment down the borehole subsequent to drilling, collecting continuous optical and acoustic images of the borehole's stratigraphy and other geophysical proxies. This study uses the cuttings and the borehole geophysical data to explore the changing environmental conditions of the early Jurassic.



Figure 2. Map of Mount Holyoke College. 300 ft ( $42.259924^{\circ}\text{N}$ ,  $072.568397^{\circ}\text{W}$ ) and 800 ft ( $42.2142^{\circ}\text{N}$ ,  $072.5714^{\circ}\text{W}$ ) boreholes indicated with yellow pins.

### *1.6 Previous Work on Campus*

The stratigraphy under the Mount Holyoke campus has been previously studied. A monograph prepared for the United States Geological Survey was completed in 1898 by Emerson on the geology of the Franklin, Hampshire, and Hampden counties of Massachusetts. In it, a series of artesian wells descriptions are included that describe the color and textural characteristics of the rocks with their associated depth, including one that was done at Mt Holyoke College. Well cuttings are described every 10 ft. A published composite based on these descriptions, descriptions of another artesian well drilled proximal to the Holyoke dam, and outcrops along the Holyoke dam railroad tracks is shown in Figure 2. Although the stratigraphic descriptions are relatively old and the exact location of the well is not specified in the report, it still accounts for the bedrock at Mount Holyoke and represents the first time that the underlying campus stratigraphy was described.



In the spring of 2016, Mount Holyoke alumnus Lorna Mei Yun Mitchinson-Field '16 did a class project on a separate 300 ft well on the Mount Holyoke campus, (Figure 2). The well is 338 m southeast of the 800 ft well and topographically 9.75 m lower. Their project had the similar goals as this study - to relate the local campus stratigraphy to the regional valley stratigraphy. The methods used by Mitchinson-Field, however, were limited to stratigraphy based on cuttings. Nonetheless, their study represented the first time that the underlying bedrock stratigraphy was documented on campus by the College's Geology department.

This study builds on the work by Mitchinson-Field (2016) by describing the lithologic changes that represent changing environmental conditions of the lacustrine bedrock on campus during the Early Jurassic. Moreover, this study utilizes both drill cuttings and borehole geophysical data to examine the role of astronomically influenced climate cyclicity in the stratigraphic transitions. It is the first study to use a cuttings based stratigraphy to measure chemical and physical proxies and produce a composite stratigraphy based on these parameters. This study demonstrates the feasibility of using well cuttings (backed up by borehole televiewer data showing the continuous borehole stratigraphy) to interpret cyclical stratigraphy of the Hartford basin.

## **2 METHODS**

### *2.1 Field Methods*

The 800 ft borehole used in this study was drilled in June during the summer of 2020 with the purpose of evaluating the geothermal potential of the rocks underlying this part of campus. The well site is located on the northern edge of the Mount Holyoke College campus (Figure 2) at 42.2142° N, 072.5714° W. The College chose this site because it is adjacent to the area that will likely be used as a future geothermal well field by the College. Skillings and Sons drilled this borehole and collected geophysical data, and a formation thermal conductivity study was presented by Hager-Richter Geosciences, Inc. in a report sent directly to the College.

#### *2.1.1 Drilling the Well*

The borehole used in this study was an 800 ft well, 6 inches in diameter and a full suite of geophysical methods were used to document the downhole stratigraphy, described in *Geophysical Methods* section below. The drilling started on June 24th, 2020 and ended on June 26th, 2020. A rotary air hammer method was used with a concave drill bit type. An 18 ft steel casing was used to isolate the well and stabilize the top of the borehole, therefore geophysical data and images of the borehole begins at the base of the casing at 20 ft. The well was drilled in 20 ft sections in accordance

with the length of each section of drill stem. The borehole was evacuated with compressed air prior to the addition of another section of drill stem (A. Werner pers. com., 2022).

### *2.1.2 Sample collection and processing*

Well cutting samples were collected by Prof. Alan Werner and Dr. Jenica Allen. The method included placing a stainless-steel colander next to the borehole to catch the cuttings that were flung-out of the borehole. They collected samples at the end of each 5-foot interval, and they maintained constant communication with the driller to ensure that the correct sample depth was collected. They rinsed the cuttings twice in bins of water and laid out on a tarp in stratigraphic order to sun-dry at the site. They collected one hundred and sixty-one (161) samples and placed them in labeled (depth in ft) Ziploc bags - in most cases around a liter of cuttings were collected, although some sample volumes were less than that. The samples were then brought back to the lab and further washed and sieved by Dr. Claire Pless with a 1.4 mm sieve to remove the mud fraction of the samples and any other debris. The cuttings were then left to fully dry in the lab in open 1-gallon Ziploc bags. This resulted in samples with cuttings that were typically 15 mm long and around 2mm thick on average (fingernail sized) (Figure 4, 5).

The cuttings document sampling of the borehole stratigraphy, integrated through each five-foot section. The absolute stratigraphic depth of each sample is uncertain because the rate of transport up the borehole is not known. Further, the

cuttings are unable to accurately document thin stratigraphic layers or abrupt stratigraphic transitions. Therefore, we expected the resulting stratigraphy (henceforth referred to as “cuttings stratigraphy”) to be somewhat offset from the true stratigraphic depth. However, because the borehole was “blown clear” at the end of each 20 ft. segment, it is unlikely that the major stratigraphic transitions between the cuttings stratigraphy and the image stratigraphy are offset by more than 20 ft and the actual depth assigned to the cuttings is thought to be within 10 ft. It is possible that deeper cuttings could be contaminated by younger borehole debris, however, the borehole’s acoustic caliper (data not shown) shows that the borehole is uniform and smooth and does not show evidence of irregularities or collapse.

### 2.1.3 Geophysical Methods

Hager-Richter Geosciences performed a formation thermal conductivity on the 800 ft geothermal test borehole. The Geothermal Resource Technologies' (GRTI) unit attached to the vertical borehole was used to document and interpret the core stratigraphy. These data were compiled from a data report sent directly to the college and through personal communications with Robert Garfield, who helped process the individual log sections of the raw data. They measured a full suite of parameters, but the parameters that were most pertinent to this study were the natural gamma ray log and the Optical Televiwer. The other parameters, although important for evaluating the geothermal characteristics of the rocks, are not as useful for the interpretation of the geologic history of the section drilled. The geophysical data have a sampling rate of 0.1 ft from 7.5 - 801.2 ft, providing a high resolution (*in situ*) record. This study uses the original driller's units (ft) to be consistent with the drilling protocols. The Optical Televiwer (OTV) data consists of high-resolution oriented camera images of the borehole starting at 19.5 ft (the bottom of the drill casing) to just above 800 ft (Hager Richter, 2020). Natural gamma ray (SI units) is used in the well logging industry to determine the in situ radioactivity of the rocks exposed in the borehole, and in other applications as a tool for determining visual correlation with other wells.

## 2.2 Laboratory Methods

### 2.2.1 Borehole Cuttings

The cuttings that were collected during the drilling operation are used to reconstruct the cuttings stratigraphy and to provide physical samples of the rock units. The cuttings consist of siltstones and mudstone deposits. The cuttings stratigraphy refers to the borehole stratigraphy as interpreted using the recovered cuttings, which were retrieved from the site during drilling and treated as described in section 2.1.2. The cuttings were arranged in a “faux core” with respect to depth in order to identify and interpret stratigraphic changes (Figure 4) and to more easily produce the cuttings stratigraphy shown later in this report. This stratigraphy shows colors ranging from red, dark-light red alternations, light gray, and dark gray. The lab processing of the samples allowed the acquisition of chemical and physical parameters including magnetic susceptibility, loss on ignition, and XRF chemical data.



Figure 4. Composite made of drill cuttings. Section shows 295 ft – 370 ft of the 800 ft record (left to right).

### 2.2.1.1 Color and Appearance

The color of the borehole cuttings, as seen with indoor lighting, consists of red, gray, and dark gray siltstone and shale. I characterized three representative samples (Figure 5) using a Munsell Soil Color Book. I also noted the texture of the sediment throughout the borehole via visual assessment of the cuttings. I used the visual, color stratigraphy to make a stratigraphic column for visual correlation with other figures.



Figure 5. Samples of drill cuttings from various depths that show differences in color of the main stratigraphic units (120ft = dark gray; 175 ft = gray; 650 ft, 600 ft = red).

### 2.2.2 *Magnetic Susceptibility*

Magnetic susceptibility (MS) is a parameter that is often used as a measure of stratigraphic variations in magnetic mineralogy in the strata, including lacustrine environments (Hilton, 1986). It is a measure of the magnetization of minerals to an applied magnetic field (Bates and Jackson, 1984). More specifically, MS measures the ratio of the strength of the magnetization response in the sediment to the strength of the applied magnetic field (Gale and Hoare, 1991). The magnetization of the sample is dependent on many factors, including chemical and mineral composition (i.e., a proxy for Iron), grain size and shape, degree of compaction, the organic matter content etc. Most importantly for this study, MS can also act as a proxy for the presence of organic matter: more organic matter in a sample decreases the measured MS due to the diamagnetic properties of organic matter (Gale and Hoare, 1991). I used this physical proxy to provide compositional information about samples that cannot be observed macroscopically.

I measured the magnetic properties of the recovered cuttings using a MS2 Bartington magnetic susceptibility meter with a MS2E High Resolution Surface Scanning Sensor attachment. Our method included gathering approximately ½ - 1 cup of each 5-foot interval sample and placing them in a plastic bowl. I pressed them down with the bottom of a beaker to reduce pore spaces between the cuttings, and then gently pressed the sensor attachment over each sample to take a reading. I pressed the sensor attachment in five locations throughout each sample for

approximately 3 seconds and recorded the highest reading. This method was done in accordance with the procedures of previous work (Mitchinson-Field, 2016).

### 2.2.3 Loss on Ignition (LOI)

I measured loss on ignition (LOI) to determine the organic matter content of each 5 ft. interval of the stratigraphy. The LOI method is generally used as a proxy for organic matter content and is a technique often applied to lake sediments and other depositional settings (Pasternack, UCDAVIS). I used LOI to determine differences in combustible materials which can be used as a proxy for changes in organic matter content.

The LOI method includes the use of a precision balance, lab gloves, small crucibles, a laboratory drying oven, a desiccant chamber, and an electric muffle furnace. I selected ~ 1 tbsp of every 5-foot interval sample and weighed them with the precision balance (error = 0.001 g) to around 6g. After weighing the sample, I placed them in crucibles and weighed them again, establishing a wet weight of the sample. I then placed the crucibles in a 150 C° laboratory drying oven for 24 hours to drive-off moisture ( $W_{dry}$ ). After weighing and establishing a dry weight of the samples, I placed the crucibles in a 550 C° electric muffle furnace for 2 hours, allowed the samples to cool in a desiccation chamber, and weighed a final time to establish a 550C° weight ( $W_{550}$ ). When the crucibles were not in the oven, they were in a desiccant chamber to

avoid the reabsorption of moisture. I calculated the percent LOI for each depth using the following equation:

Equation 1: Solution for calculating LOI%

$$LOI\% = (W_{dry} - W_{550}) / (W_{dry} - W_{Crucible}) \times 100 \quad (1)$$

All LOI methods were followed according to the SFU Soil Science Lab instruction manual (Robertson, 2011).

#### 2.2.4 X-Ray Fluorescence

X-ray fluorescence (XRF) is a method of determining the abundance of inorganic elements in geologic materials. Short wavelength X-ray radiation is used as the energy source. The incident electromagnetically radioactive, high energy X-ray photons then stimulate the secondary, lower energy X-ray photons from the sample's atomic structure (Bruker Handheld LLC Corporation, NA). The fluorescent energy comes from the outer electron orbitals replacing the inner electron orbitals and releasing energy in the process. The energy differences between outer and inner electron orbitals are characteristic of each element, so the fluorescent X-rays resulting from this process can be used to determine specific elements in each sample.

I gathered the XRF data at Columbia University's Lamont-Doherty Earth Observatory campus, in the lab of Dr. Paul Olsen under the guidance of Clara Chang.

The data were generated from the borehole cuttings, and the resulting depth scale is in ft. Although the XRF method generally calls for the grinding of the samples (Olsen, pers. com., 2021), time constraints did not allow me to follow this part of the protocol. Instead, I packed the raw samples (cuttings) into XRF analysis cups, covered them with mylar film, and measured them using a Bruker Tracer 5 Portable XRF Spectrometer. I used the gun's "GeoEXPLORATION" Mode, which first takes an initial reading to determine the general composition of the sample (a matrix of coefficients for each element is also constructed, which allows inter-element interferences to be accounted for). The count rate for each element is normalized, and the sample is measured two more times to obtain a final abundance percent by comparing known concentrations to the corresponding adjusted normalized count rates (Kenna et al., 2011). The output is interpreted in ppm (Chang, pers. com., 2022), and so the resulting measurements were output in parts per million per the company's proprietary factory calibration. These multiple measurements also result in an error output for each element at each depth and represent a combination of detector uncertainties and matrix corrections. This mode is able to measure elements ranging from Sodium to Uranium, on the default 90 second count time. As such the results are considered a semi-quantitative analysis of the samples. Optimally, standard reference material would be used to perform external calibration (Kenna et al., 2011). However, this step was not used in this method as it was not necessary because I was interested in relative changes through the borehole, not quantitative concentrations. In the

future, a matrix matched calibration with standard reference material could be conducted to determine elemental concentrations (Chang, pers. com., 2022).

#### *2.2.4.1 Elements used in XRF*

The use of XRF analysis on borehole drill cuttings and the analysis of the resulting chemistry is not a method that is traditional in the literature for exploration of cyclicity (Olsen, 2022, pers. com.). However, understanding the behavior of elements in paleo-lake sediments, specifically resulting from changing redox conditions, can aid in further understanding the environment of deposition.

For this project, I decided to focus on Uranium (U), Sulfur (S), and Iron (Fe) relative abundances. Uranium, a radioactive element, can be correlated with the natural gamma ray log measured in the borehole, which is used for the statistical analysis in this study. Uranium in lake deposits occurs at the sediment-water interface in reducing lake-bottom conditions (Turner-Peterson et al., 1985). Sulfur is present as a sulfide under reducing conditions, such as in pyrite ( $\text{Fe}_2\text{S}$ ) (Serfes et al., 2010), and as a sulfate in gypsum ( $\text{CaSO}_4 \cdot 2\text{H}_2\text{O}$ ) and possibly other sulfate minerals under oxidizing (evaporitic) conditions (Serfes et al., 2010). Fe is important in relation to S, but also as an abundant element throughout the borehole in general.

### 2.2.5 *Acycle Software*

The *Acycle v2.3.1* time series analysis program was developed by Mingsong Li from Peking University and Linda A. Hinnov from George Mason University and runs using the MATLAB programming language. The software was developed to streamline time series analysis in the geosciences, specifically for paleoclimate research. The program also offers an array of objective methodologies to determine paleoclimate signals (Li et al, 2019). Using this software's tools, specifically the unsmoothed periodogram and *TimeOpt* methods, I am able to determine the frequencies of statistically significant sedimentation cycles and the sedimentation rate of our 800 ft stratigraphy using the natural gamma ray log data (raw data illustrated in Figure 5) retrieved from the borehole geophysical report. I converted the natural gamma ray log data to meters as per the program's specifications, resulting in a 243-meter-long stratigraphy.

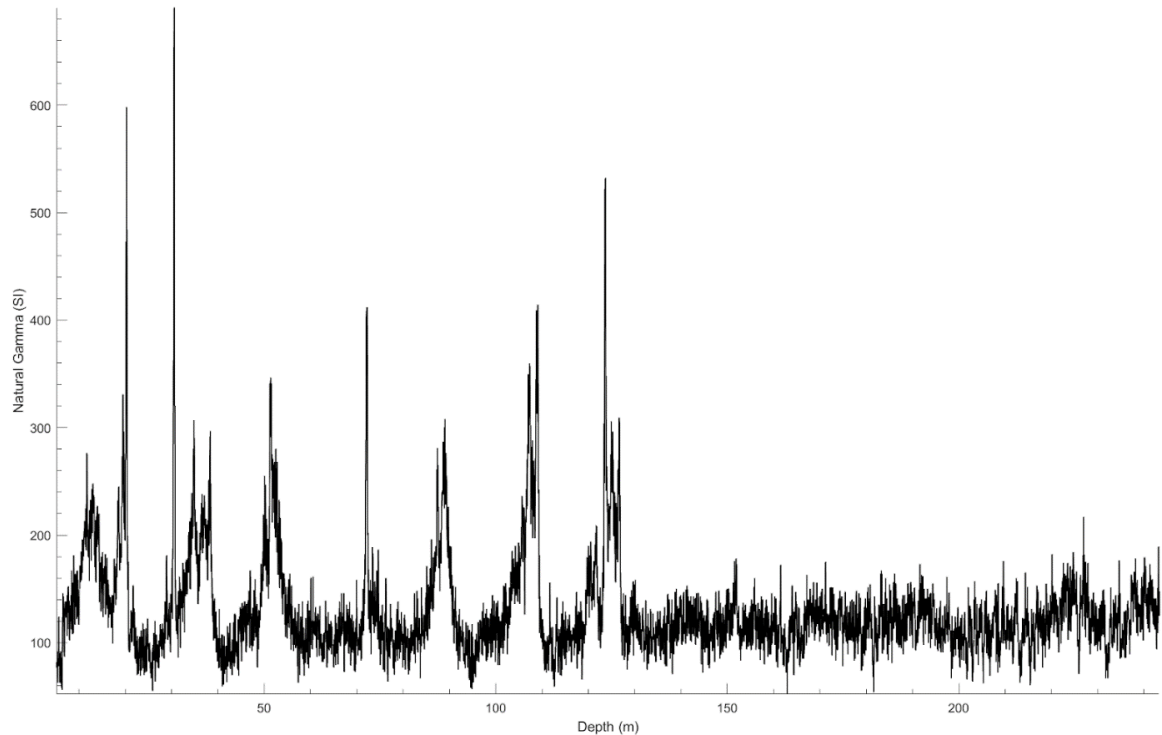


Figure 6. Natural Gamma ray log (SI) raw data. Data taken every 0.1 ft down the borehole.

I interpolated the data (rate = 0.03048) within the program to determine a uniform sampling rate in meters, which is a requirement for the fast Fourier function and *TimeOpt* solutions. The issue in doing this interpolation is that it creates data that does not exist in the original dataset. After comparison of the original and interpolated dataset, it was found that the interpolation added 3 extra values to the dataset, indicating that interpolation was appropriate and did not greatly alter the data.

### 2.2.5.1 Sedimentation Rate and Power Spectral Analysis

I evaluated the periodicity of the stratigraphy in two ways: first by assuming a sedimentation rate for this section in accordance with the sedimentation rate that has been published in the literature (0.9m/kyr, Sha et al., 2015), and then by use of fast Fourier function in *Acycle*. The first method considers the published sedimentation rate, relates it to the OTV data, and determines that cyclical frequencies are present in the visual stratigraphy under this sedimentation rate.

The “spectral analysis” (power spectral) component of *Acycle* is used to recognize periodic characteristics in the time series input using various forms of Fourier analysis, where the magnitude of the variation in the data is interpreted as a function of frequency (a version of the Fourier series). For my data, I used the “Periodogram” function (unsmoothed fast Fourier function) in *Acycle*. A periodogram allows me to determine the dominant cycles in a time series, as seen in the example in Figure 7. The goal is to determine significant frequencies and periods in the data by taking the inverse x-axis value of the most dominant peaks in the periodogram output (1/frequency). The higher amplitude a peak in the periodogram is, the more variance in the original data for which it accounts. With these frequency values, I can establish time-frequency relationships in the depth data which, with additional assumptions regarding uniformity in sedimentation rate, can convert the data into thousands of years (time) using data in meters (depth) with the *TimeOpt* method below.

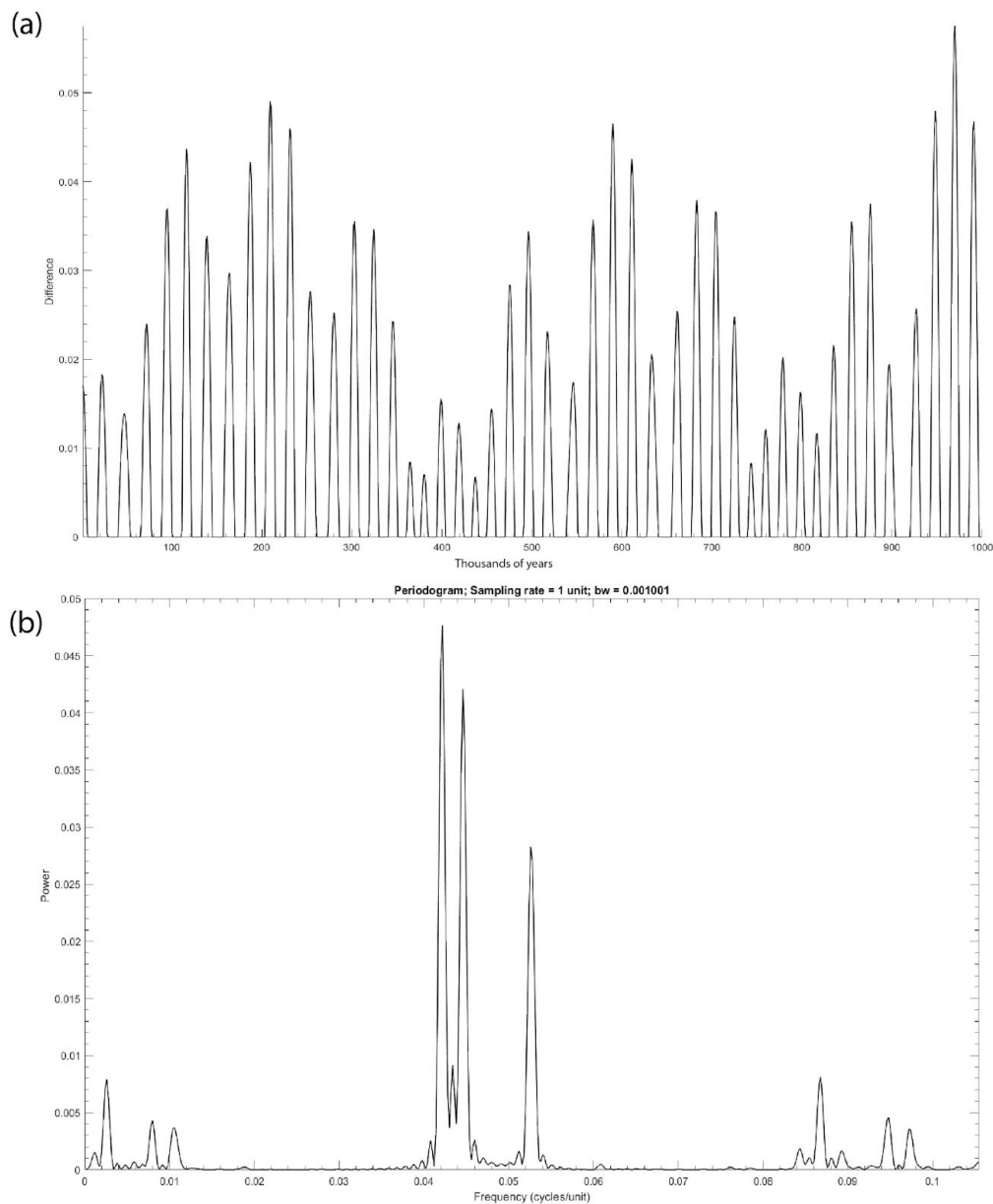


Figure 7. (a) Astronomical solution for differences in precession frequencies as determined by Laskar et al (2011, LA10a). The time series was clipped at the mean value to allow Fourier analysis to express the modulation of precession, which would otherwise be invisible. (b) Corresponding periodogram with peaks indicating powerful frequencies detected in (a). The periodogram's highest peak is at 0.042, whose inverse is  $1/0.042 = 23.81$ , indicating that the most important cycle in this series has a period of 23.81.

### 2.2.5.2 TimeOpt Analysis

*TimeOpt*, short for time scale optimization, is a data-driven method developed by Stephen Meyers which combines probabilistic linear regression models with known and projected eccentricity and precession values in an attempt to reveal astronomical signals (Meyers, 2015). This time series solution is incorporated into *Acycle*. *TimeOpt* identifies a series of models constructed from the data that best fit the assumption of Milankovitch pacing. The results also provide information on the difference between any possible astronomical signal and noise is accounted for by comparing an envelope of the maximum amplitude values with reconstructed models.

*TimeOpt* also outputs an optimal sedimentation rate that is determined by the optimized equation:

$$r^2_{opt} = r^2_{envelope} r^2_{spectral} \quad (2) \text{ (Meyers, 2015)}$$

Where  $r^2_{opt}$  is the model strength at the optimal sedimentation rate determined by  $r^2_{envelope}$  and  $r^2_{spectral}$ . Here,  $r^2_{envelope}$  is determined by the amplitude of the natural gamma ray log data series (extracted using Hilbert transform and band-pass filtering) multiplied by default eccentricity periods (Meyers, 2015). Then,  $r^2_{envelope}$  uses an equation that multiplies the product of the amplitude values of the data series and

predetermined eccentricity periods at different sedimentation rates, finding the best fit for the data at each sedimentation rate. The other component of equation (2),  $r^2_{spectral}$ , is a somewhat similarly determined equation that generates a correlation factor between the data and pre-established astronomical parameters. Also, the amplitude of the data series is not used in  $r^2_{spectral}$ , but rather the data series itself, resulting in a spectral power series (Meyers, 2015). The fit is determined between the data series and the astronomical model series. Equation (2) takes into consideration a combination of complementary approaches to yield an optimal sedimentation rate that can be used to interpret the depth series (m) into time (kyr). Graphical representation of model fit, sedimentation rate, and reconstructed model and data comparisons are included in the *TimeOpt* output.

An important limitation of *TimeOpt* in *Acycle* is that only eccentricity and precession values are used in the model, obliquity is not. However, the data in this report do not present obliquity components due to the subtropical paleo-latitudes (~12-24 °N). Obliquity cycles (40 kyr) may appear in some equatorial geologic records but considering the good fit of the *TimeOpt* method with this data, there does not appear to be an obliquity component in this record.

### **3 RESULTS**

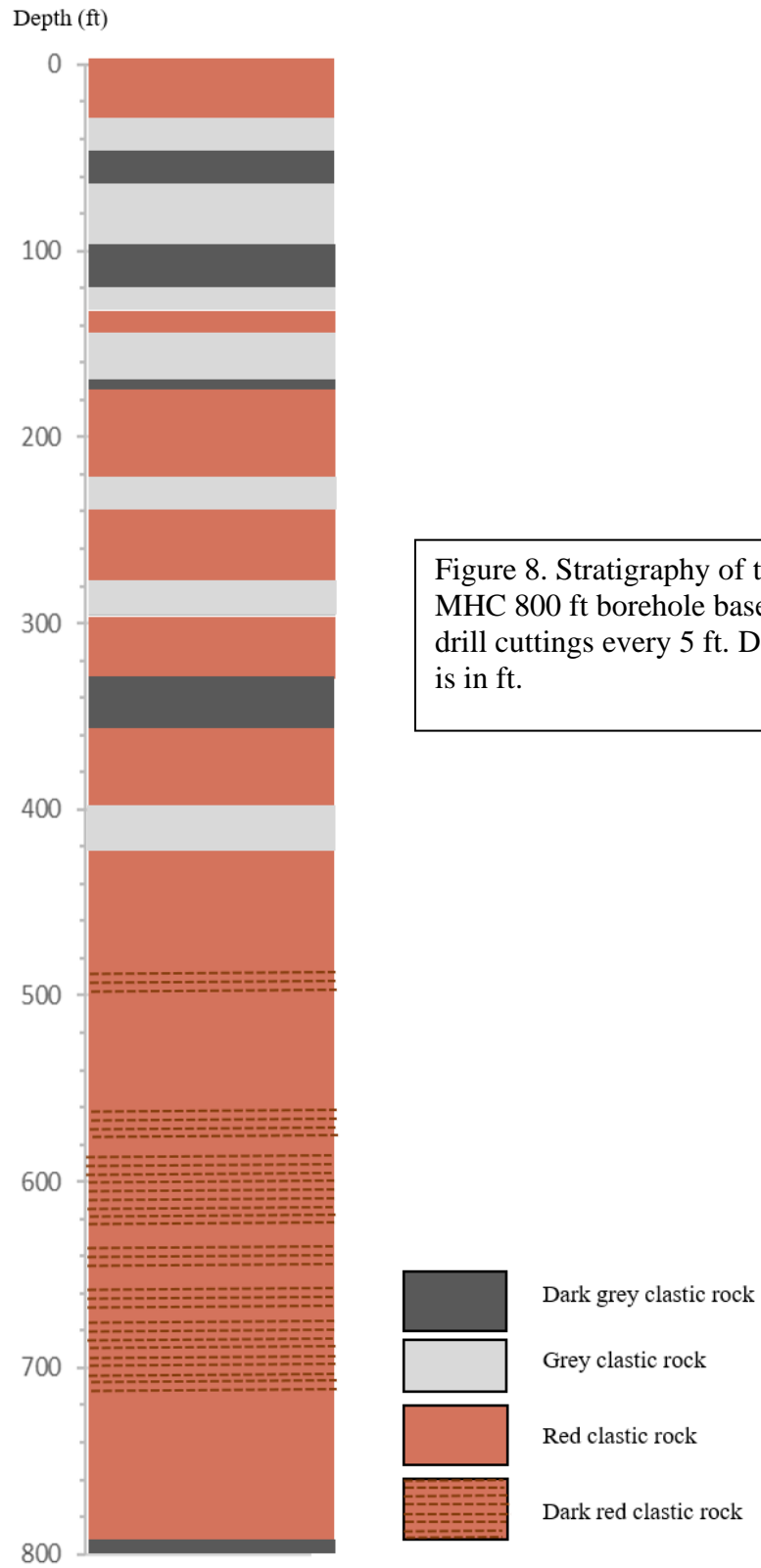
#### *3.1 Cuttings stratigraphy results*

The borehole stratigraphy interpreted from the drill cuttings shows mostly red mudstones with interbedded gray and dark gray units that are texturally consistent and lack any notable textural changes (Figure 8). Dark gray cuttings are GLEY2 2.5/5PB on average; gray cuttings are GLEY1 5/N on average; and red cuttings are 10R 3/2 and 10R 3/1 on average (Figure 4). Two red samples were chosen to illustrate the slight heterogeneity seen in the 'red' category, which is discussed further later in this report. These colors tend to be uniform - that is, there is little or no mixing of reddish and gray-ish cuttings in the selected samples. The dark gray cuttings have visible pyrite inclusions and below 400 feet, some of the reddish cuttings have gypsum inclusions and they are confined to the darker red facies. These inclusions only occur in the lower 400 ft of the stratigraphy.

There are seven gray sections in the upper half of the stratigraphy, some of which are accompanied by light gray sections (at ~100 ft and ~140 ft) and some are just light-dark gray sections (at 220 ft and at 400 ft). From 30 ft - 130 ft, there is a light - dark - light - dark - light gray section with no red sections in between. Besides this portion of the stratigraphy, all gray sections are approximately 20 - 25 ft thick.

The contacts between the sections are abrupt with little to no mixing of the cuttings. The red sections between the gray sections do not vary much in color and are approximately 40 ft thick from 180 ft to 400 ft in the stratigraphy, but they're thinner in the upper section of the stratigraphy. The gray sections do not appear again below 400 ft except in one sample close to 800 ft.

The red stratigraphy below 400 ft. has a uniform red color. The light red and dark red sections appear between 500 ft and 700 ft and they are variable in thickness. There is also no uniform spacing between the sections. An important characteristic of the red section below 500 ft is that there are visible pieces of gypsum attached to the cuttings (Figure 9).



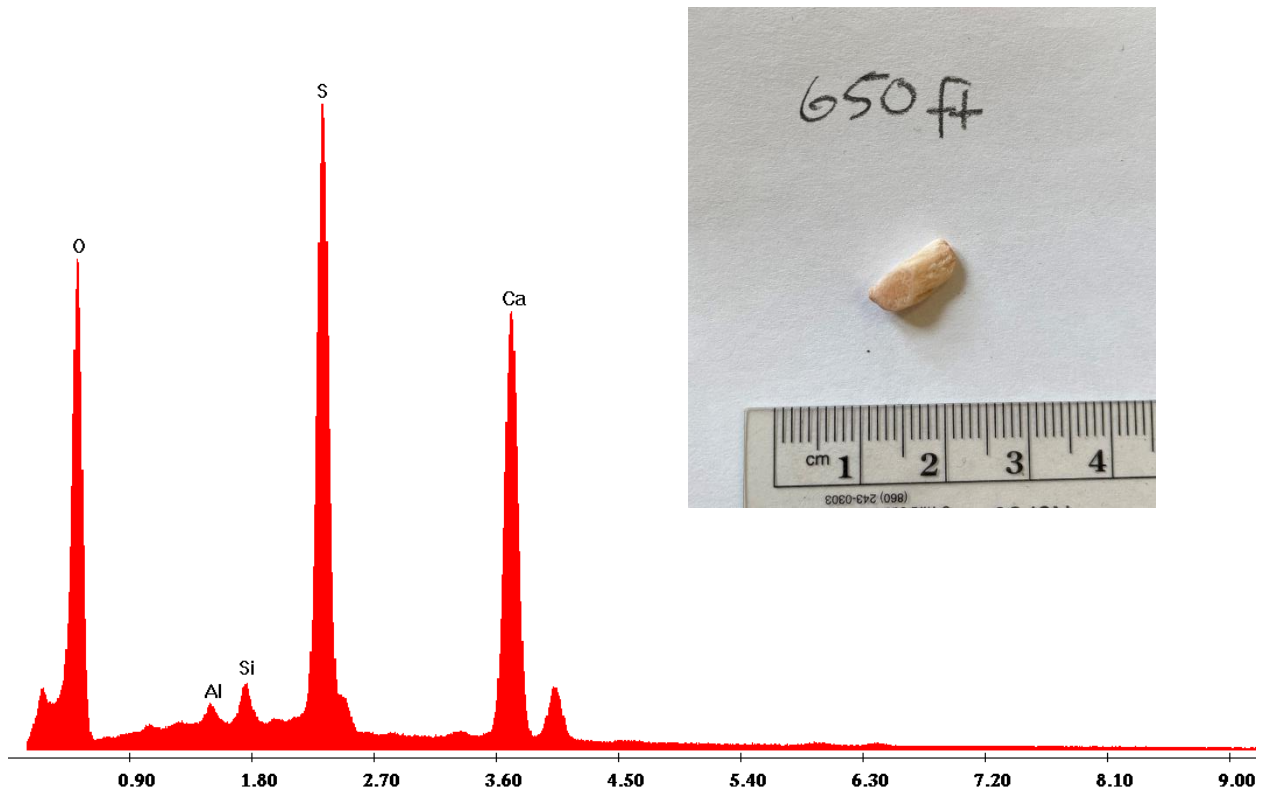


Figure 9. Gypsum from drill cuttings found at 650 ft and associated SEM output.

### 3.2 OTV Stratigraphy

The OTV (Optical Televiewer) stratigraphy provides a high-resolution continuous image of the *in situ* borehole stratigraphy. Unlike the cutting stratigraphy, which is taken at 5 ft intervals and includes the unknowns of transport to the surface and possible mixing with cuttings from shallower depths, the OTV images provide a high resolution (< 1cm) record of the borehole stratigraphy with an accurate depth scale (Figure 10). Most of the borehole consists of red shale/siltstone but does contain thinner units of gray to dark gray shales that are about 20-25 ft in thickness and occur in the upper 400 ft of the stratigraphy. The first two sections of gray bedding (at approximately 30 ft and 115 ft) are darker than the rest of the gray sections. Between these gray sections there are sections of red bedding, and the thickness of these sections is variable, ranging from 35 to 40 ft on average

Below 400 ft, there is an absence of gray bedding. Between 400 ft and ~550 ft, the red bedding is homogeneous. Below 550 ft to the base of the borehole, there is a sharp difference between red bedding that matches the color of the upper part of the red bedding stratigraphy and a red bedding that is several shades darker. The spacing between the red bedding and the dark red bedding in the lower portion of the stratigraphy is variable, and there are numerous alternations between the two colors. The dark red bedding contains traces of interbedded gypsum, as seen at around 800 ft in Figure 10 and more clearly in Figure 11. At 800 ft, the stratigraphy starts to shift to a gray section (Figure 10).

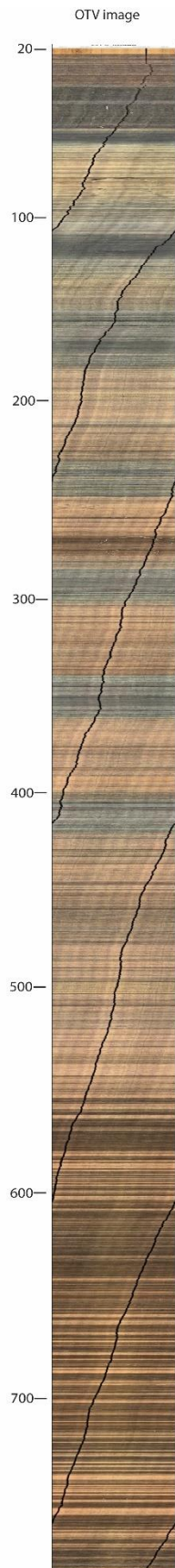


Figure 10. OTV image of the MHC 800 ft borehole. Depth is in ft. The image is overlain by a dark line that occurs five times and is an artifact without geological significance. According to the field geophysical technician, this represents either a crack in the camera lens or an issue with the digital camera (Werner, pers. comm., 2022).

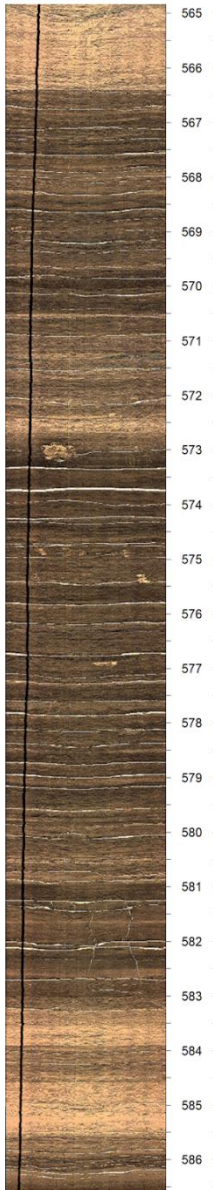


Figure 11. Zoomed-in image of the 565-586 ft section of the OTV stratigraphy. Gypsum presence is denoted by the thin white lines along the dark red portion of the stratigraphy.

### *3.3 Magnetic Susceptibility*

The magnetic susceptibility values range from a low of 6 to a maximum of 84 SI and shows a decrease in the range of measurements with depth (Figure 12). Most of the variability occurs in the upper 600 ft of the stratigraphy; the lower 200 ft is relatively constant. There is a missing value at 285 ft due to a missed sample during the collection of cuttings (A. Werner, pers. comm., 2021). The peaks present in the upper 400 ft have, on average, a spacing of 25 ft. There are 3 significant MS peaks between 0-200 ft., and 3 less apparent peaks between 200 - 400 ft. The low MS values similarly have an interval of approximately 25 ft. There are 2 peaks (below 40 SI) between 600-800 ft. Overall, there is a negative trend of MS with depth.

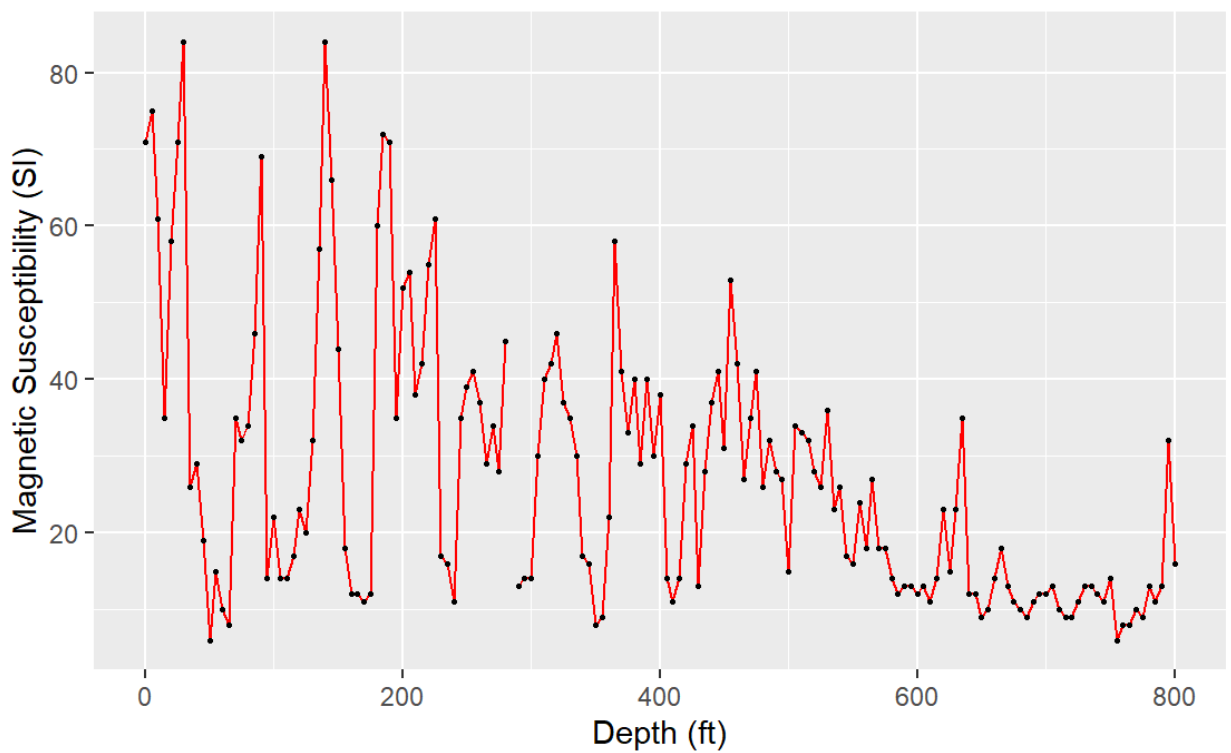


Figure 12. MS (SI) vs depth - measured on borehole cuttings.

### 3.4 Loss on Ignition

The LOI data ranges from ~0.2% (500 ft) to ~5.6% (115 ft) (Figure 13). The maximum peaks in these data occur mostly in the upper 400 ft, more specifically between 0-200 ft. The LOI is less variable from ~150 - 300 ft and after 400 ft. There are peaks at 45-65 ft, 115-120 ft, 345 ft, and 800 ft. The 800 ft “peak” is not a complete peak, but an upward trend is apparent. These peaks are supported, on average, by 8 data points (40 ft). There is a missing value at 285 ft due to a missed

sample during the collection of cuttings (A. Werner, pers. Comm., 2021). Overall, there is no obvious trend of LOI with depth.

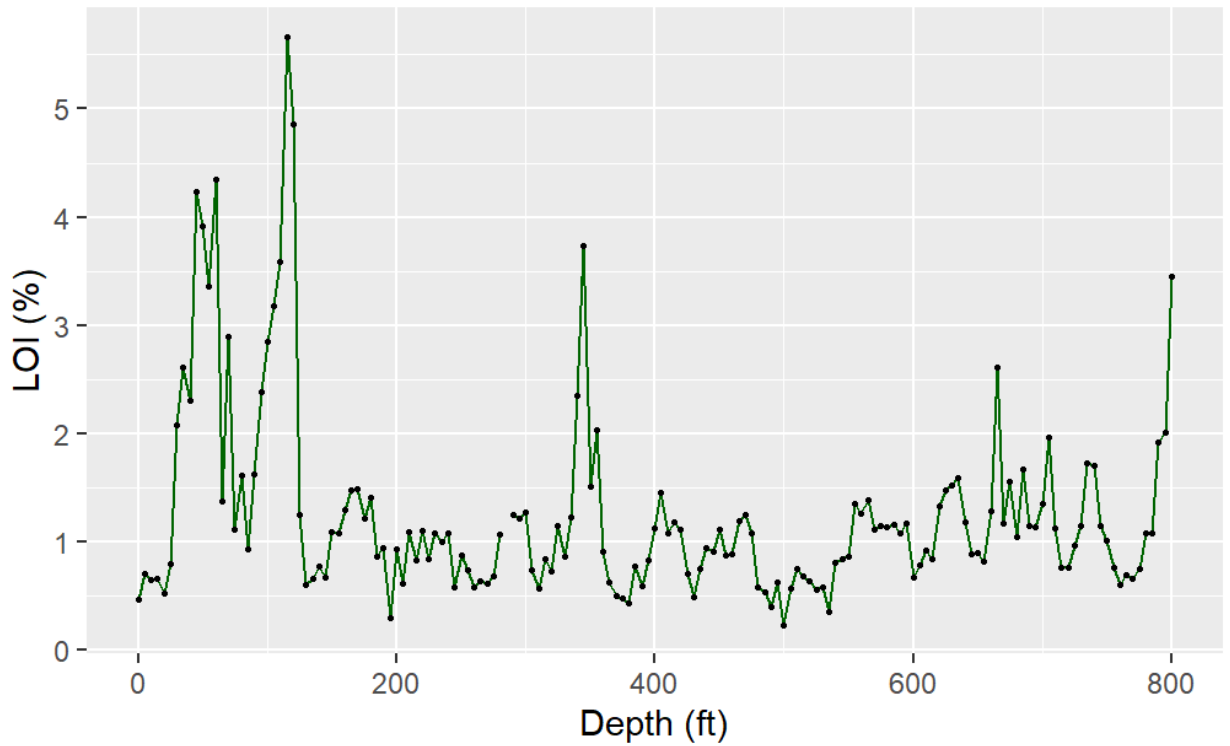


Figure 13. LOI (%) vs. depth – measured on borehole cuttings.

### *3.5 XRF Results*

#### *3.5.1 Uranium*

The relative concentrations of U in the cutting samples are relatively low (Figure 14). Most outputs by the pXRF sensor had “NA” readings, interpreted here as zeroes in the data. The non-NA data points are found mostly on the upper 400 ft of the borehole. The majority of the measurements do not go above 0.005 ppm, indicating constant concentrations of U down the length of the borehole. The spacing between data peaks in the upper 400 ft of the borehole is about 40 ft on average, and some of the peaks are supported by more than one data point. The highest measurement occurs at 415 ft, which measures 0.0187 ppm of U. There are only two small U peaks between 400-800 ft.

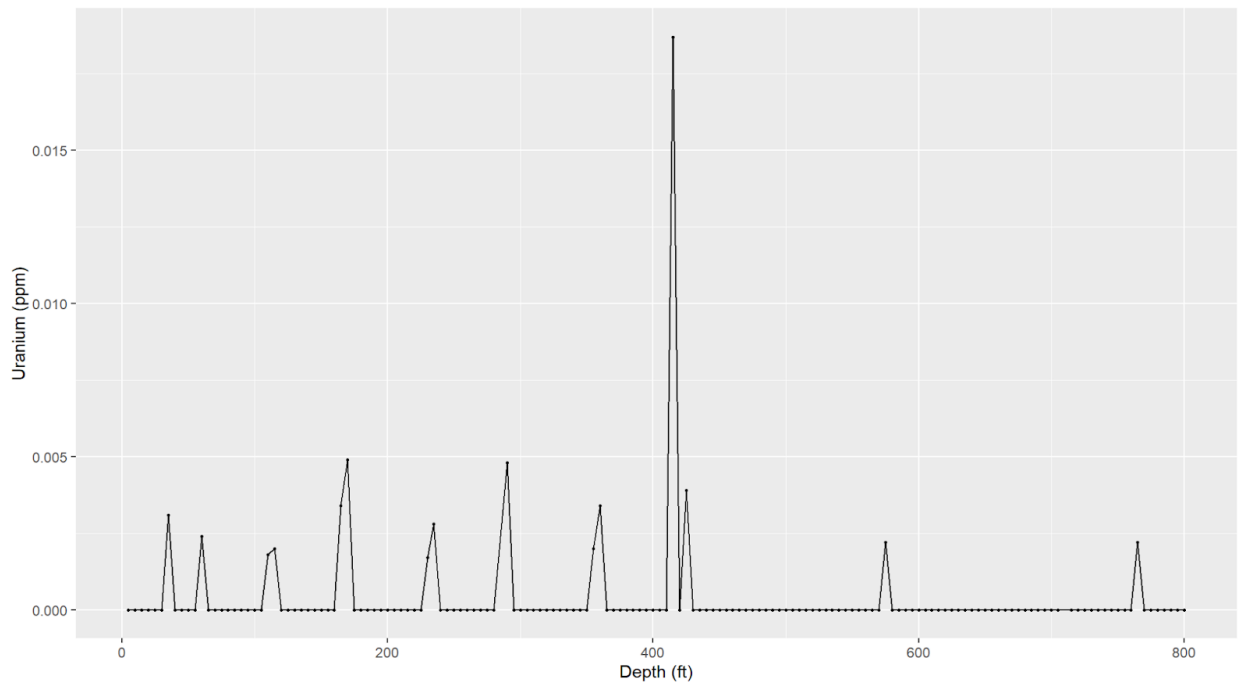


Figure 14. Relative U concentrations (ppm) vs. depth measured on cuttings.

### 3.5.2 Sulfur

Sulfur content of the cuttings ranges from near zero to over 5 ppm (Figure 15). Three sections of variable Sulfur concentrations occur in the stratigraphy, at the beginning (20-180 ft), the middle (350-420 ft), and the end of the data (580-800 ft). The upper interval has four peaks that reach 3ppm and have constant spacing between them. The middle interval has two peaks that reach 2ppm separated by 50 ft. After these two peaks, there is an interval that lacks abundant Sulfur between 450-550 ft - this interval is significantly constant in its near-zero Sulfur concentration. The lowest

interval has more dramatic activity, with several peaks rising above 3 ppm and two peaks reaching 5 ppm. In total, there are 9 zones of relatively high Sulfur activity between 600-800 ft. There is no observable trend in the S that aligns with depth, as there are two zones of elevated values above 200 ft and below 600 ft.

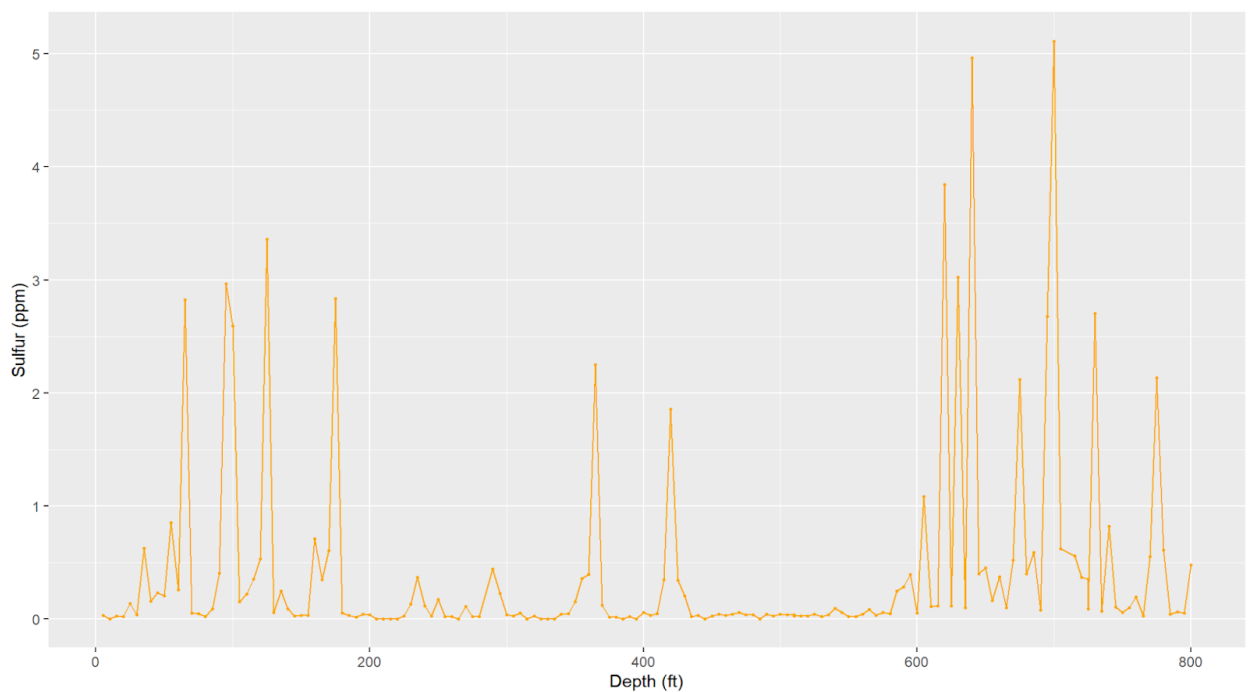


Figure 15. Relative Sulfur concentrations (ppm) of the cuttings.

### 3.5.3. Iron

Iron concentrations are quite variable throughout the borehole (Figure 16), and there is no obvious trend in the data. Unlike Sulfur and Uranium, the variations in Iron do not appear to be periodic in nature, and there are no obvious ways to distinguish specific segments that align with specific depths in the data as in other proxies. Iron does not reach near 0 values very often and is the most abundant element (reaching 6 ppm) out of the three considered in this study.

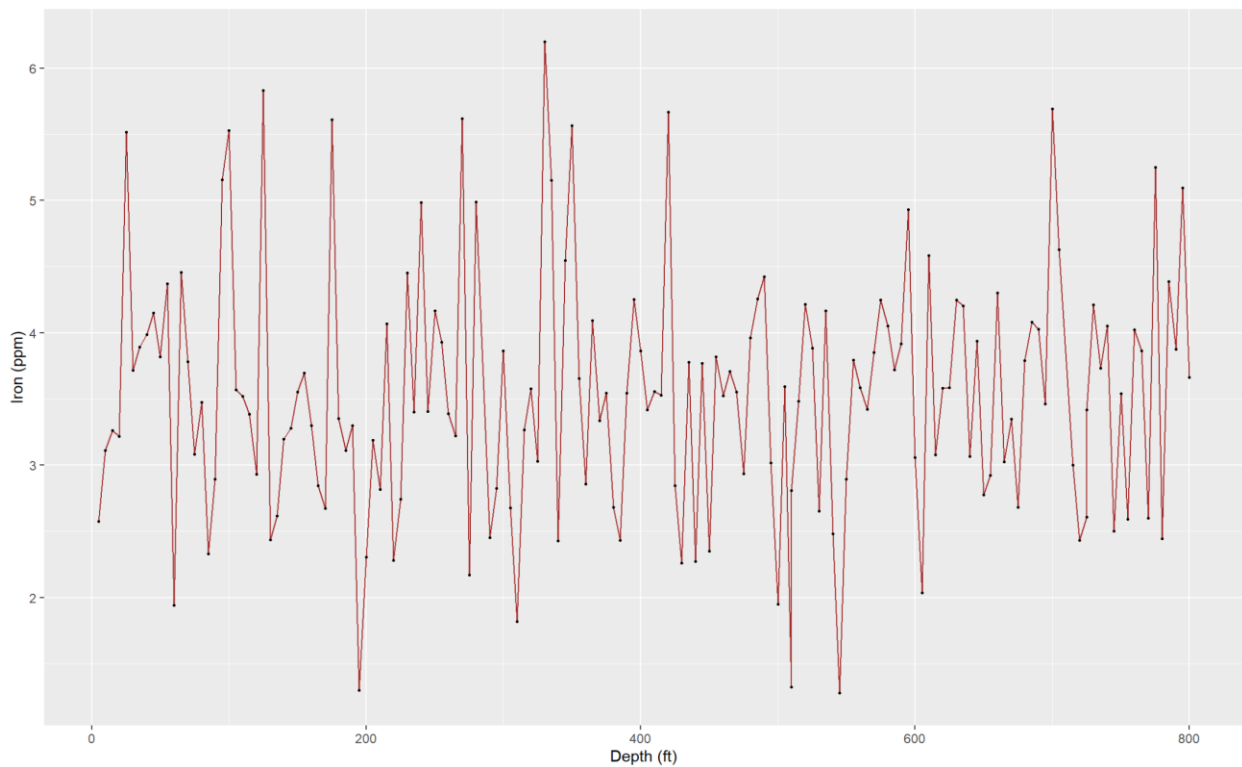


Figure 16. Relative Fe concentrations (ppm) of the cuttings.

3.6 Statistical Analysis based on Natural Gamma ray

As observed in previous proxies in this report, the stratigraphy appears to have periodic cyclicity that is visually and chemically present in the upper 400 ft of the borehole (Figure 10, 12, 13, 14, 15). The periods are so clear, in fact, that the frequency can be visually determined using the OTV image:

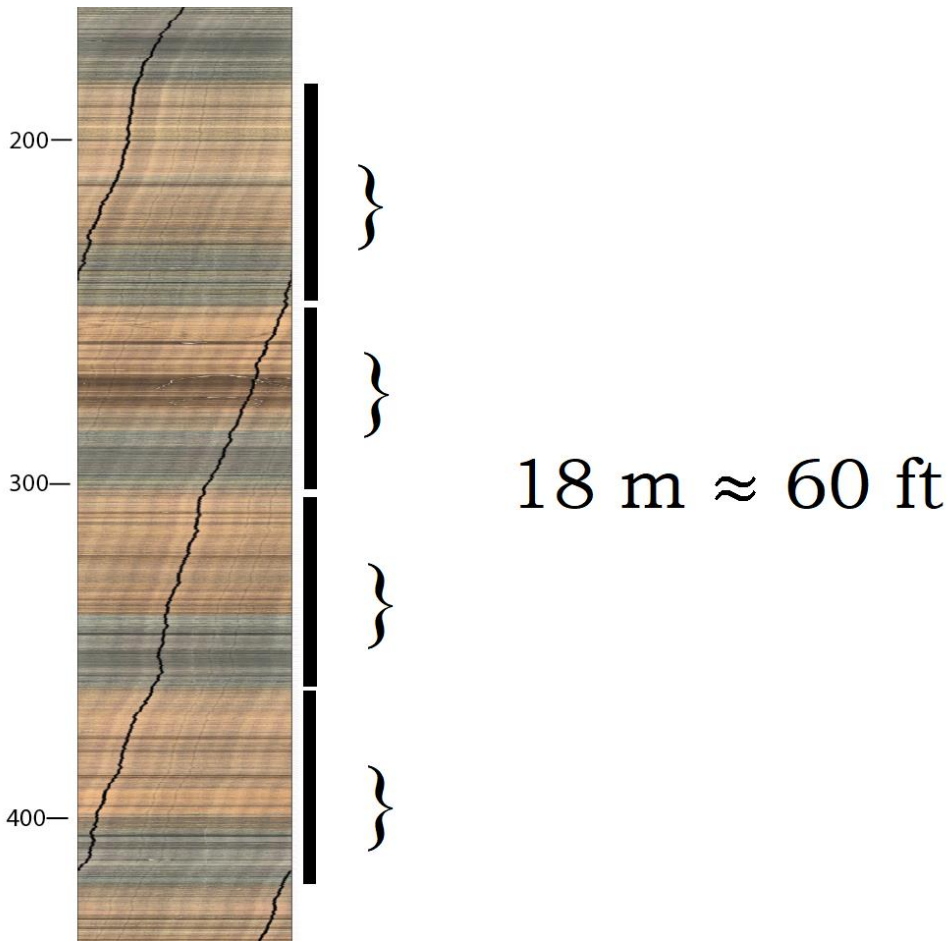


Figure 17. Visual assessment of the periodicity down the borehole, frequency = 1 cycle/18 m on average.

This method of visual assessment gives an average cyclicity of 18 m when the published sedimentation rate of 0.9m/kyr is applied, with each cycle having a length of 16.2 thousand years (kyr). However, the visual method is subjective and prone to human error, and the published sedimentation rate might not exactly agree with the actual, average sedimentation rate for the data in this study. To further refine this periodicity, fast Fourier Transform analysis and the *TimeOpt* method can give more accurate results by statistically identifying the periods in the data and then relating them to the cycles in Milankovitch forcing. The main assumption that is needed for these statistical methods is that the sedimentation rate of the data be uniform, as an uneven sedimentation rate would provide an erroneous interpretation of the environment of deposition. The sedimentation rate for the North American rift valleys has been determined to be relatively uniform and is around 1 meter of deposition every 1000 thousand years (1m/1kyr) on average (Kent and Olsen, 2008), and more accurately for the Portland formation of 0.9m/kyr (Sha et al., 2015). Therefore, we expect that with the refined statistical methods to measure periodicity, the sedimentation rate will approximate the value that is established in the literature.

### *3.6.1 Periodogram/Spectral analysis*

The spectral analysis (fast Fourier Transform, here presented as an unsmoothed periodogram) of the natural gamma ray (raw data in Figure 6) log shows few to no peaks at higher frequencies but does show strong peaks at 0.0025, 0.044, 0.057, and 0.11 (Figure 18). The highest power peak (A) represents a value of 0.057

on the x-axis, whose inverse corresponds to a period of 17.5. Therefore, the Fourier Transform suggests periodic cyclicity in the data that is repeated approximately every 17.5 m. There are three subordinate peaks that show power, at (B) 0.0025 ( $1/0.0025 = 400$ ), (C) 0.044 ( $1/0.044 = 22.73$ ), and (D) 0.11 ( $1/0.11 = 9.10$ ). The subordinate peaks suggest cyclical activity approximately every 400 m, every 22.73 m, and every 9.10 m.

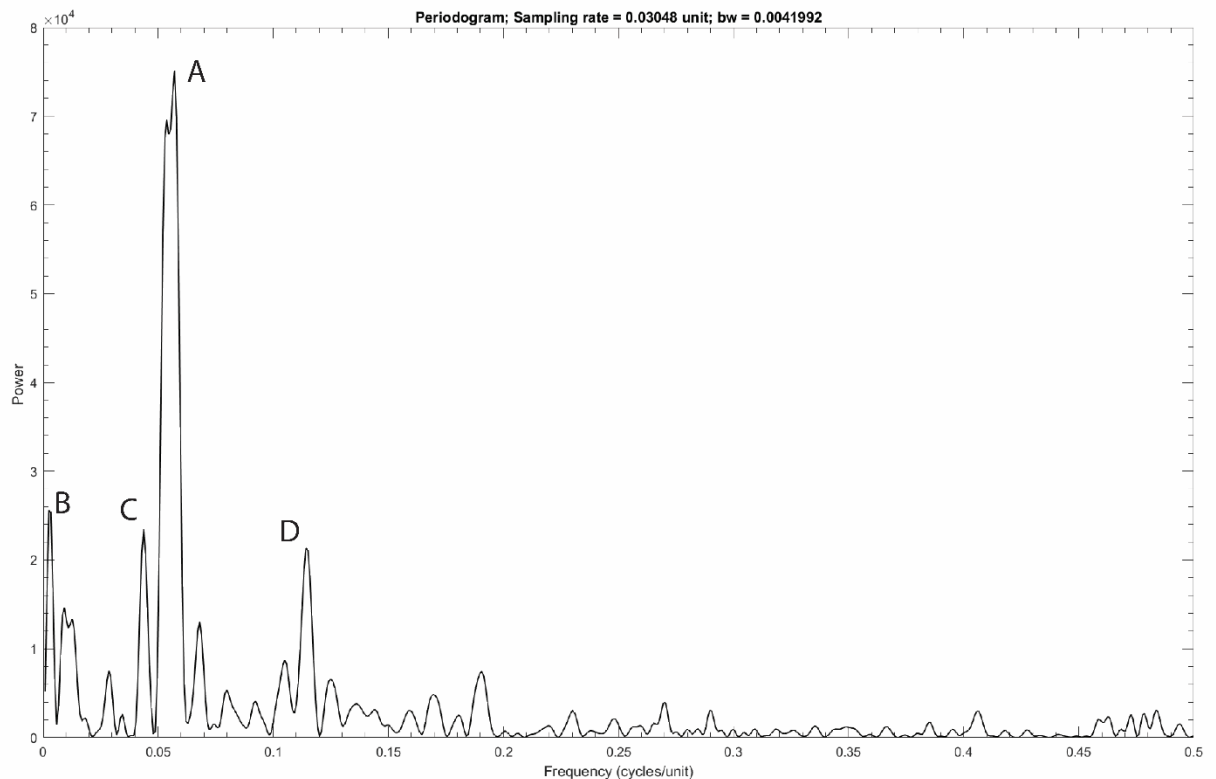


Figure 18. Periodogram estimates of the MHC borehole natural gamma ray log data (max frequency = 1). High power period value (A) corresponds to  $1/0.057 = 1$  cycle/17.5 m.

### 3.6.2 TimeOpt

The *TimeOpt* method performed the calculation for 400 simulations with sedimentation rates ranging from 0.0039 m/kyr to 2.00 m/kyr. The maximum  $r^2_{envelope}$  (approx. 0.9), occurred at a sedimentation rate of 1.86 cm/kyr, and the maximum  $r^2_{spectral}$  (approx. 1.0) occurred at a sedimentation rate of 0.18 m/kyr (Figure 19(b)). The combined approach (equation 2) yields a sedimentation rate of 86.9791 cm/kyr ( $r^2_{opt}$  approx. 0.15) (Figure 19(a)). The fit of the predetermined precession and eccentricity frequency values with the data derived periodogram is shown in Figure 19(f), where the values around 0.05 have a good fit with the periodogram (same as Figure 19). The goodness of fit between the eccentricity derived equation used to calculate  $r^2_{envelope}$  with the time calibrated model using the optimal sedimentation rate is shown in Figures 19(c) and 19(d).

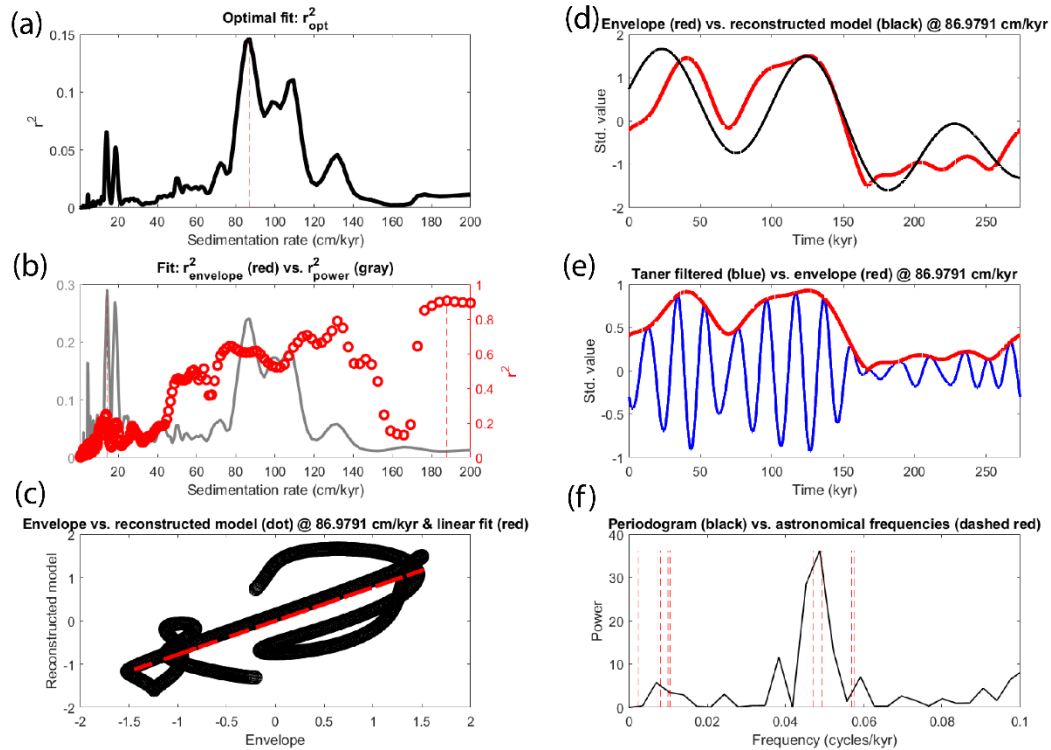


Figure 19. TimeOpt analysis of the MHC borehole natural gamma ray log data. (a) Combined envelope and spectral power fit ( $r^2_{\text{opt}}$ , black) dashed red line indicating specific sedimentation rate (86.9791 cm/kyr). (b) Squared Spearman correlation coefficients ( $r^2$ ) for the amplitude envelope fit ( $r^2_{\text{envelope}}$ , red) and spectral power fit ( $r^2_{\text{spectral}}$ , gray). (c) Cross plot of the data amplitude envelope and the TimeOpt reconstructed model, red dashed line is 1:1 fit. (d) Comparison of the data amplitude envelope (red) and the reconstructed model from  $r^2_{\text{envelope}}$  from equation (1) using the optimal sedimentation rate. (e) Comparison of the Taner filtered data using the optimal sedimentation rate (blue) and amplitude envelope determined by Hilbert transform (red). (f) Periodogram of the natural gamma ray log data, given the sedimentation rate output in (d). Precession and eccentricity astronomical target periods are in dashed red.

## **4 INTERPRETATIONS**

### *4.1 Correlation of Cuttings and OTV image*

The borehole OTV image stratigraphy and the cuttings stratigraphy share striking similarities in the order, thickness, and positioning of the main stratigraphic units (Figure 20). The composite image is shifted approximately 20 ft., as the collection of cuttings started at 0 ft and the OTV image software started recording the borehole stratigraphy at 20 ft. Therefore, the sections that are compared between both records correspond to 20 - 800 ft of the stratigraphy.

The relationships between the red, gray, and dark gray facies in both records compare remarkably well and there doesn't appear to be more than 5 ft of offset. All the gray and dark gray facies in the OTV image are recognized in the cuttings log. The visual correlation is improved when the cutting stratigraphy is shifted up a few feet relative to the borehole stratigraphy. The exception to this pattern is the gray section at 400 ft, which is almost in line but shifted slightly downwards in the composite image. This could point to a "calibration" in the lag between the collection of the samples used to make the composite image. An alternative interpretation could be that, coincidentally, the mixing in the samples that make up and surround the 400 ft gray section in the cuttings stratigraphy align well with the OTV image stratigraphy. Additionally, the contacts between the red and dark gray facies in the

OTV image appear abrupt in nature, suggesting that the abrupt contacts present in both stratigraphies are real contacts down the borehole. The visual correlations appear robust, suggesting that geochemical data from the cuttings can confidently be related to absolute borehole depth. The lower 400 ft of the stratigraphy is also reflected in both records. Below 500 ft, the observed dark-red sections in the cuttings match up quite well with the dark-red sections in the OTV image in regard to their position. Yet not all occurrences of the dark-red sections are accounted for in the interpreted cuttings stratigraphy, especially below 700 ft.

The slight differences between the records notwithstanding, the interpretations I have made of the corresponding sections are visually compelling. Therefore, the data gathered from cuttings (MS, LOI, and XRF) is compared to the geophysical data (OTV image, natural gamma ray log) without accounting for any major inconsistencies between the two records. This comparison also shows the viability and utility of using cutting stratigraphy for continuous stratigraphic interpretations, at least for shallow (<1000 ft) wells.

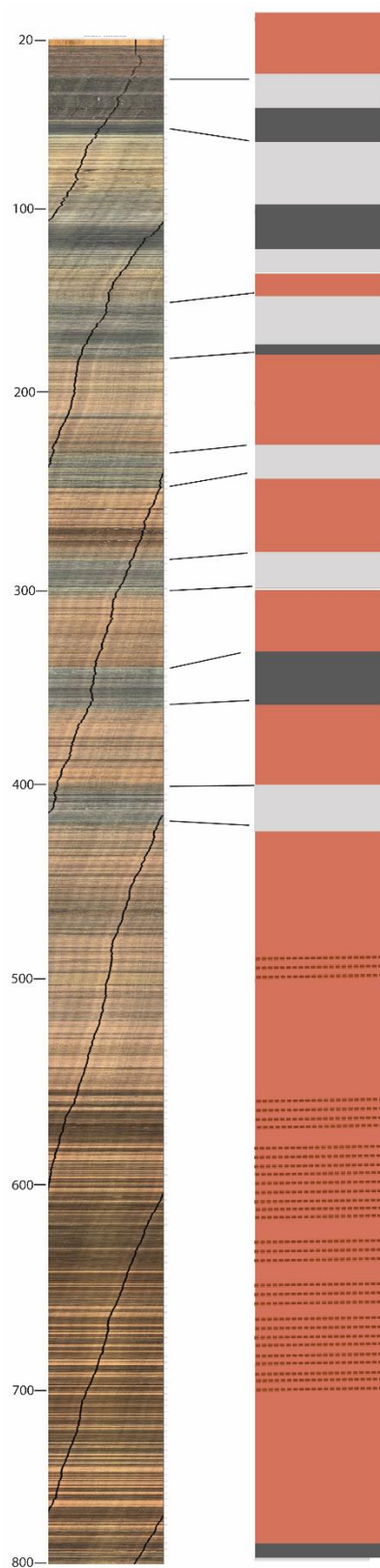


Figure 20. OTV borehole image (left) and borehole composite image (right) based on cuttings. Borehole composite image shifted upwards approx. 20 ft. Diagonal line on the OTV image is an imperfection on the camera lens.

#### *4.2 Magnetic Susceptibility and Loss on Ignition*

The MS and LOI records are generally inversely matched (Figure 21). This is especially evident in the upper 400 ft of the data. From 0 - 200 ft, when LOI is high MS is low. Conversely, when LOI is low MS tends to be high. The lows and highs are also significantly different from the rest of the variability in the data (ANOVA, data not shown). The relationships of the extremes in the LOI and MS data can also be associated with the dark gray sections in the borehole (Figure 22).

Below 200 ft. the inverse, visual correlation of the two parameters is less distinct. For example, there is a noticeable low in the MS data at 240 ft, but there is no corresponding peak in the LOI data (Figure 21). The missing data point at around 280 ft appears to be part of a decrease in the MS data, and the same data point seems to correspond to a small peak in the LOI data. Due to the incomplete and ambiguous nature of the two instances described in the data, no correlation with a black line is indicated. However, at around 350 ft, the inverse correlation is apparent again. Below 400 ft it is difficult to correlate the two proxies as there are no obvious highs and lows in the data, impeding an accurate visual correlation between the two records.

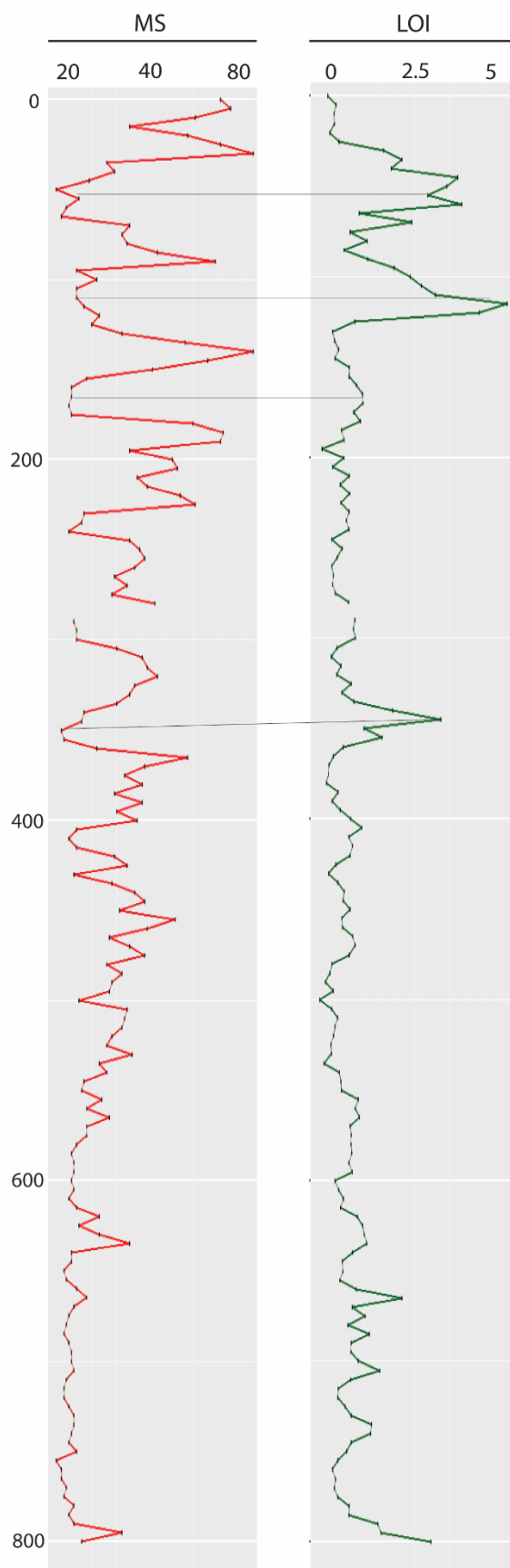


Figure 21. MS (red) and LOI (green) record comparison. Correlations are indicated with dark gray lines.

The major variations in the data are correlated to the dark gray shales (Figure 22). Because the grain size is fairly constant throughout the borehole, the variation in chemical composition and organic matter are what mostly explain the amplitude variation in MS. In particular, MS peaks are likely driven by elements with a greater magnetic moment that are being reflected by the MS sensor's magnetic field, like hematite. Another contribution to the variance in MS is the amount of organic matter present in the samples. Organic matter tends to be paramagnetic (Gale and Hoare, 1991), so its presence cancels out the magnetic field applied by the MS sensor resulting in a low value. Therefore, the presence of organic matter, may explain the low MS values. On the other hand, organic matter presence also explains the peaks in the LOI curve, as the difference between samples before and after ignition is partly dependent on the amount of organic matter in the samples. Sections with more organic matter will have a higher loss on ignition percentage and will therefore have lower MS values.

The MS and LOI values below 400 ft are interesting, as the curves are no longer inversely related. However, they are not exactly in phase either - the relationship between the records is hard to distinguish as the data becomes more "muted" below 400 ft. MS and LOI values exist below 400 ft, but it is not clear what exactly they are related to in the visual stratigraphy (Figure 22). Regardless, it appears that in the lower interval of the stratigraphy, changes in LOI are not associated with changes in MS like they are in the upper part of the stratigraphy.

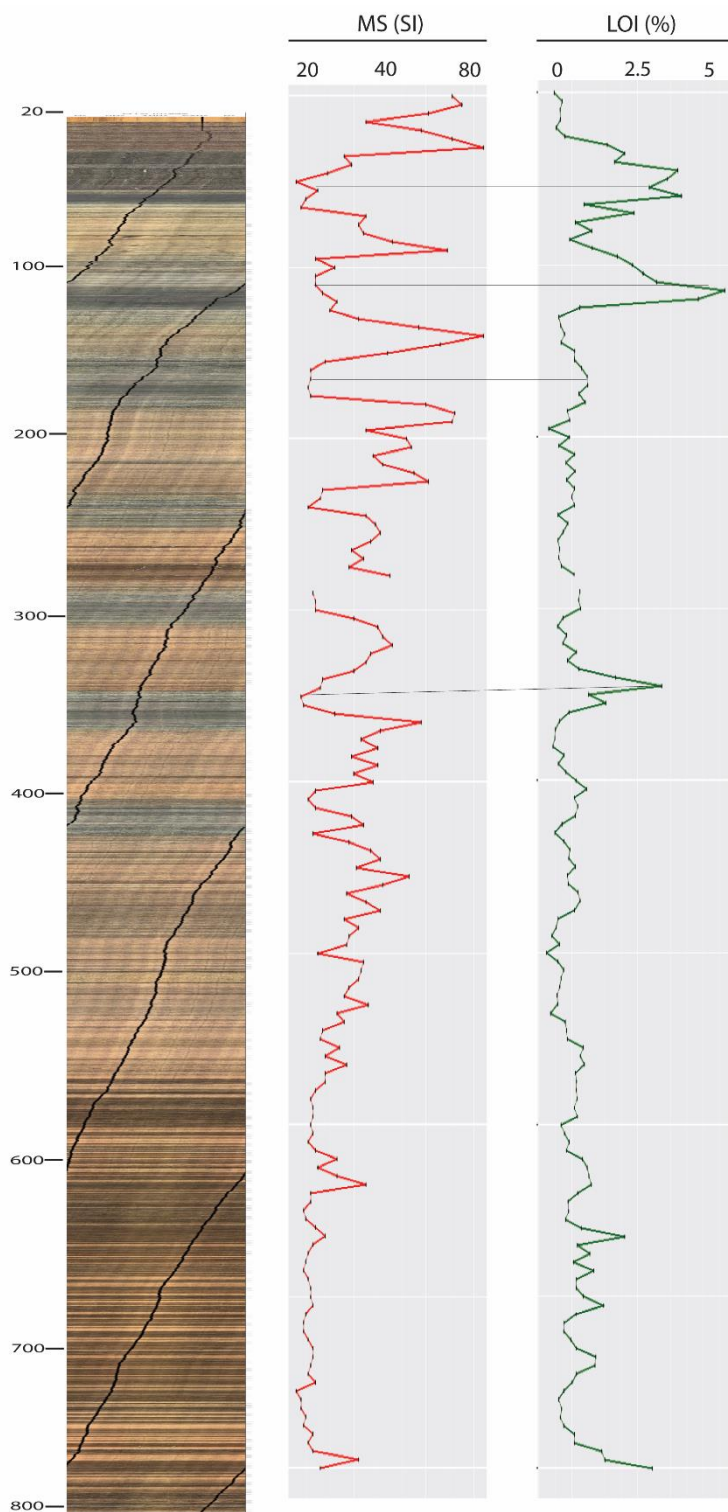


Figure 22. Borehole OTV image, MS (red), and LOI (green) record comparison. Correlations are indicated with dark gray lines.

### *4.3 X-Ray Fluorescence analyses*

#### *4.3.1 Uranium*

For the elemental data, the existence of slow-moving groundwater flow might have influenced the existence and migration of some elements that were deposited millions of years ago, and thus the chemistry found with this method is carefully interpreted. The XRF data chosen for analysis relate to the redox changes in the paleo-lake environment and for further correlation with the natural gamma ray log in the case of Uranium (U) (Figure 23). Much like the OTV image, the natural gamma ray log does not give a complete record of the stratigraphy, but rather records natural radiation from 17.5 ft to 801.2 ft. down the borehole (Hager Richter Geosciences, 2020). Therefore, the U was correlated accordingly by moving the record 20 ft upwards for a proper comparison. The U peaks correspond remarkably well with the natural gamma ray log peaks (Figure 23). As U is a radioactive element, the variation in the Thorium and Potassium, which can also influence the natural gamma ray log, were preliminarily measured. They were present in small amounts in the cuttings but did not correlate well with the natural gamma ray peaks (data not shown). After reviewing other radioactive elements that have the potential to affect the natural gamma ray log, U appears to be the principal driver of the natural gamma ray, despite its low relative abundance in the rock cuttings.

The U peaks are mostly constant in value throughout the record, and the maximum U high at 400 ft also lines up with a high in the natural gamma ray record.

The two small U peaks below 400 ft do not line up with peaks in gamma radiation, suggesting potential contamination of the sample. The natural gamma ray record has many high values which make up the peaks that correspond to the U, and the highest natural gamma ray values happen toward the end of the peak before abruptly dropping back to near 0 values.

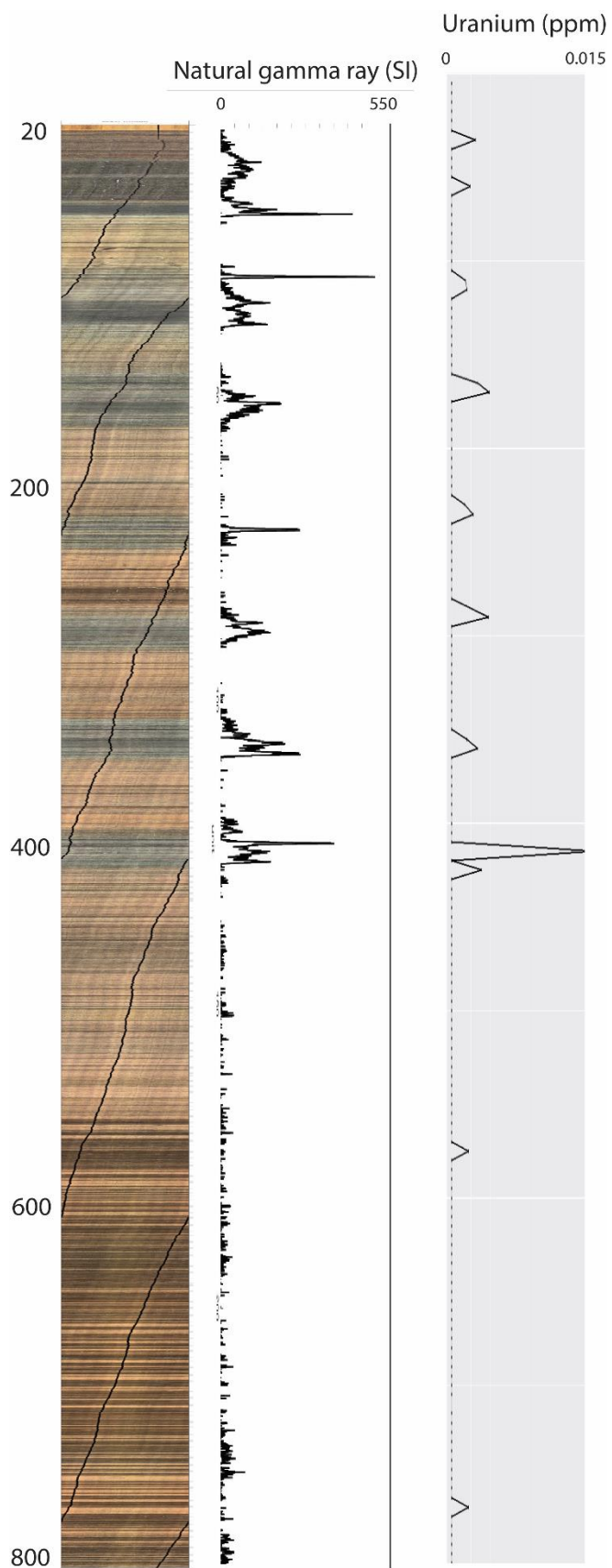


Figure 23. Comparison between the U relative abundance in rock cuttings (ppm) and the natural gamma ray log from borehole drilling (SI units).

#### 4.3.2. Sulfur & Iron

The correlation of the coinciding Fe and S peaks and the occurrence of 1mm pyrite ( $\text{FeS}_2$ ) at those intervals suggests reducing lake-bottom conditions (Figure 24). The relative abundance of Sulfur in the stratigraphy is interpreted to be forming sulfide and sulfate compounds. This is apparent when comparing the S relative abundances to the Fe output of the pXRF sensor (Figure 25). The S highs towards the top of the stratigraphy correlate with high Fe peaks, especially between 0 and 200 ft. The occurrence of pyrite between 200 and 400 ft, as well as immediately below 400 ft, also align with the Fe, although less obviously so. This accounts for seven S highs in the upper section of the stratigraphy, which align with the 7 dark gray shale units in the imaged stratigraphy of the borehole (Figure 25).



Figure 24. Pyrite crystals (1mm) in the dark gray shale on US penny. Shale chip is about 1 cm in length.

The interval of low Sulfur between 450 ft and 550 ft is associated with a constant red interval in the OTV image (Figure 25). The S peaks below 400 ft are associated with gypsum flakes that are visibly present in the borehole images and in the cuttings (Figure 26). Curiously, the Ca relative abundance does not correlate with the S relative abundance of the borehole cuttings after 400 ft. (Ca data not shown), although gypsum is present in the lower half of the stratigraphy (Figure 11). After Scanning Electron Microscope (SEM) analysis of a gypsum flake found in the cuttings, I confirmed that the white mineral in the cuttings is, in fact, gypsum (Figure

9). The lack of gypsum in the XRF record can be attributed to a homogeneity issue – as the samples were not powdered, the likelihood that the XRF would have measured the Ca in the gypsum is low since its detection window is small ( $<1 \text{ cm}^2$ ) (Chang, pers. comm., 2022). More representative (powdered) samples might have accounted for the low Ca. This also shows that Ca is mostly present in the gypsum flakes and less in the cuttings themselves. Regardless, high S is associated with the dark red sections of the lowermost part in the borehole. While it is difficult to correlate the dark red sections to specific S high peaks, the randomness of S highs after 500 ft tracks with the variably spaced dark red intervals.

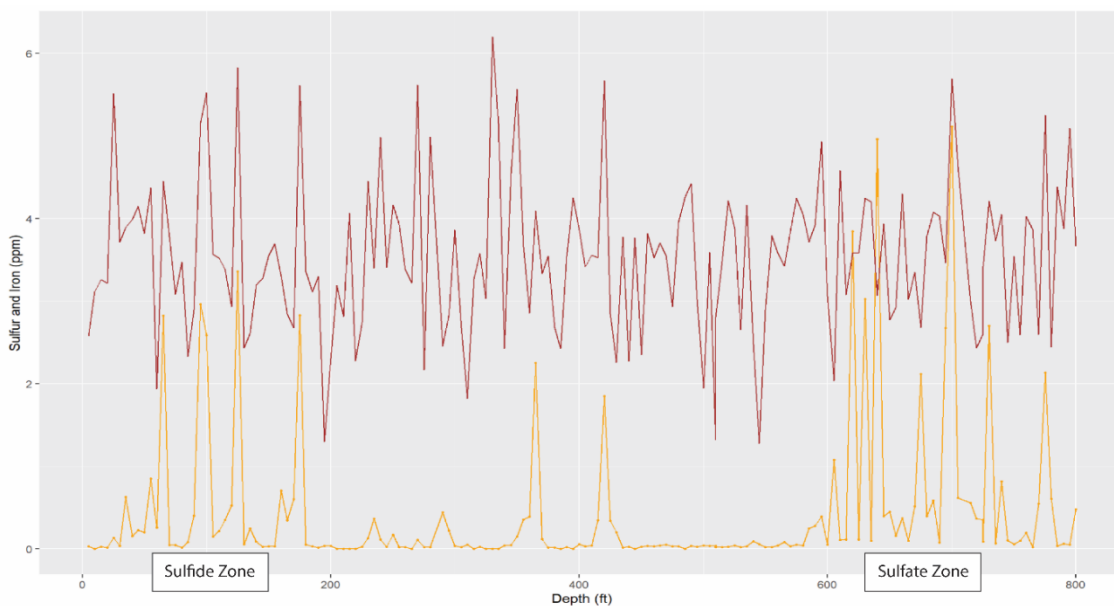


Figure 25. Comparison of the S and Fe relative abundances down the cutting stratigraphy.

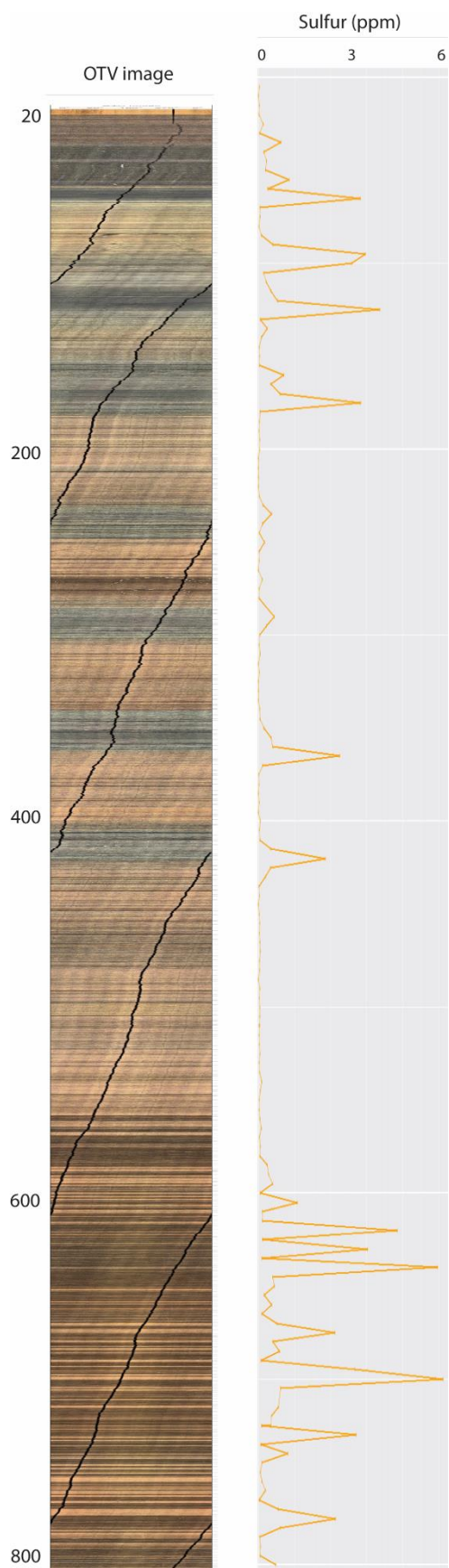


Figure 26. Comparison of the S relative abundance curve with the OTV image.

#### 4.4 Statistical Interpretation

The spectral analysis of the gamma ray data shows that there are multiple cycles in the borehole stratigraphy. The periodogram output suggests that there is evidence of a cycle happening every 400 feet, which is interpreted as more or less thousands of years (400 kyr). This is consistent with a Milankovitch eccentricity cycle of 405 kyr (Laskar, 2020). This is also reflected in the *TimeOpt* figure (e) and (d) (Figure 19), where the envelope shows large variations in the upper half of the stratigraphy. Additionally, Figures 19(d) and 19(e) suggest that the upper half of the stratigraphy is highly influencing the detection of these cycles by *TimeOpt*.

The most significant cycle that occurs down the stratigraphy shows a cyclicity of 17.5 m. This value, along with the nearby value of 22.73, is consistent with a Milankovitch precession cycle of 20 kyr (Laskar et al., 2004, Yang et al., 2020). The data driven method developed by Meyers, 2015 and employed in this study (*TimeOpt*) indicates that the sedimentation rate needed to achieve this solution is approximately 87cm/kyr. While the  $r^2$  value of the optimal sedimentation rate is not 1 or -1, this  $r^2$  relative to other paleoproxy studies of astronomical significance is sufficient based on the amount of noise in the raw data (Meyers, 2015). For example, the optimal sedimentation rate for an insolation solution established by Laskar et al 2004 yields an  $r^2$  of 0.6 (Figure S1). Moreover, the  $r^2$  value from this study is appropriate as seen in Figure 19(d), where the raw amplitude envelope data is compared to the reconstructed model that uses this sedimentation rate. When

converting the frequency values into periods from the fast Fourier transform (Figure 18), we obtain  $17.5 * 87 \text{ cm/kyr} = 15.23 \text{ cm/kyr}$ , and  $22.73 * 87 \text{ cm/kyr} = 19.78 \text{ cm/kyr}$ , which also approximates precession, especially the second calculation. The average sedimentation rate of the Portland formation has been established as being between 0.9 - 1 m/1kyr (Kent and Olsen, 2008, Sha et al., 2015), which is very similar to the 87cm/kyr value and is consistent with the difference in the distance between the sites where the data were acquired. The two precession values described above are also reflected in the TimeOpt output (Figure 19(f)), where the power spectrum maximum peak is bounded by two target astronomical frequencies. With this sedimentation rate, we can determine the number of years that are encompassed in the borehole by dividing the length of the borehole in m (243.84 m) by the sedimentation rate (0.87 m) to get a value in kyr. This amounts to a timespan of 280.2 kyr being expressed in the borehole stratigraphy.

The fit of the *TimeOpt* method for the paleo-proxy record of natural gamma ray, for 400 simulations, is considered robust, as evidenced by the lack of severe noise in Figure 19(c) and the approximation between the reconstructed model and the data series amplitude values in Figure 19(d). This claim is also supported by Monte Carlo simulations done with the data (Figure S2,  $p = 0.0000$ ). As precession and eccentricity values are embedded in the method, the correlation between the data and the predetermined astronomical solutions is present in the stratigraphic record.

#### *4.5 Environmental Interpretation*

The visible shifts in color present in the borehole and cuttings stratigraphy are cyclical in nature. The color changes (red, gray, and dark gray) observed in the stratigraphy are interpreted as changes in lake depth over geologic time, where red shales represent relatively shallow lake level conditions, and the dark grey shales represent relatively deeper lake level conditions. This interpretation is supported by a combination of the LOI, MS, and XRF proxies described in this report.

MS is likely being driven by the elemental and organic matter content changes down the borehole as opposed to variation in grain size (section 4.2). A connection can then be established between the environment of deposition, the chemistry of the rocks, and the corresponding magnetic susceptibility. When the magnetic susceptibility is high during the red intervals (Figure 22), the presence of paramagnetic or ferrimagnetic material is present in these intervals is suggested, likely in the form of hematite which gives the samples their red coloration. Although Fe is constantly high throughout the borehole, diamagnetic materials such as organic matter may be canceling out the available magnetic moment in the black shales (Gale and Hoare, 1991). Organic matter in the data can also be explained by the changing environmental conditions, where lake deposition during the dark gray intervals was associated with more organic matter deposition/preservation. The LOI peaks corresponding to the dark gray shales in the record (Figure 22), are interpreted to contain more organic matter than the red shales. Because LOI can be influenced by

other factors such as water held in the lattice of clay minerals, I cannot rule out that some of the LOI peaks may be due to other factors as well. The lack of LOI peaks in some of the dark gray shales is likewise curious (e.g., the section immediately below 400 ft). The MS data is slightly offset with the red shales at this depth, complicating the relationship between the two proxies. Below 400 feet, the behavior of the MS and LOI data suggest the existence of fundamentally different lacustrine environments over time. This environment is associated with low LOI and is interpreted as a shallow water lake environment. The presence of gypsum in the lower section of the stratigraphy suggests oxidizing conditions resulting in higher magnetic susceptibility values (Gale and Hoare, 1991), but especially in the gypsum containing sections, the MS measurements are low (Figure 22). The amount of gypsum could theoretically reduce the measured MS in this section, however the amount of gypsum in the samples was not quantified and this interpretation is therefore conjecture.

Uranium and its associated natural gamma activity is also a sensitive proxy of environmental conditions. An important characteristic of these data is that the U mobilization is seen in the natural gamma curve. As explained in section 4.3.1, U is likely to be the principal driver of the variation in the natural gamma ray log, and the highs in the U relative abundance line up well with the highest peaks in the natural gamma ray log (Figure 23). Uranium is mobile under oxidizing conditions and immobile under reducing conditions, and the occurrence of Uranium in the stratigraphy is therefore interpreted as a proxy for anoxic conditions. This interpretation is supported by the occurrence of euhedral pyrite found within the dark

gray units (Figure 24). The large Uranium peak in the last dark grey section of the upper 400 ft is interpreted to be caused by a lack of homogeneity in the sample when being measured with XRF. To confirm that the height of this peak is real, I would perform the XRF measurements again under a different protocol.

Although Sulfur and Iron levels exist at similar levels throughout the stratigraphy, the existence of pyrite in the dark gray layers and gypsum in the red units below 400 feet suggests profoundly different environmental conditions (Figure, 25). Pyrite forms in shale under reducing conditions with stable sulfide and Iron concentrations (Serfes et al, 2010). I observed that pyrite is especially abundant in the dark gray unit at 120 ft. than in other dark gray units, which might suggest subtle differences in reducing environments (dark gray units).

The red beds in the upper section of the stratigraphy have very low S measurements (Figure 25, 26). In other studies where S is used as a stratigraphic proxy, low S concentrations were interpreted as coming from eroded coal, which occurred as fluvial conditions in lacustrine environments (Chou, 2012). In the case of this study, changing basin systems can be related to changing S levels. Closed basin – shallow water conditions in the Jurassic lake environment would imply the presence of evaporites, but this is not necessarily true – for the red beds in the upper section of the stratigraphy, closed basin conditions combined with sufficient precipitation events (rain, intermediate monsoon strength) to prevent evaporite deposition would have allowed for more mobile conditions and reduced Sulfur deposition. The literature on

using S as a geochemical proxy in lacustrine conditions of Mesozoic records is not extensive (Ding et al., 2016), and there are other chemical interactions between other elements to consider as well that are beyond the scope of this research.

The red beds in the lower part of the stratigraphy, however, do have high Sulfur peaks that are not evenly spaced, much like the uneven spacing of the dark red beds in the image stratigraphy (Figure 25). These S abundances are physically related to the evaporite minerals (gypsum) present in the physical cuttings of the borehole (Figure 9, 26) and suggest evaporative environmental conditions that would have allowed for the precipitation of such evaporites. The gypsum present in these sections come from primary deposition (Bout, pers. com., 2022). These grains make up about < 20% of the stratigraphy, and the grains range from 1-5 mm in length (Figure 9). The argument for a closed basin is applicable here as well, where in this case a closed basin would have sufficient aridity that sulfates would have been able to deposit in the sedimentary record (Figure 25). The red facies represent closed basin conditions, but the red beds with low S measurements represent non-evaporitic conditions and the red beds with higher S measurements represent evaporitic conditions.

The cycles that occur down the borehole align well with the proposed Milankovitch values of precession and eccentricity (Figure 19 c, d, e, f). The periodicities of Milankovitch orbital forcing have been associated with changes in the amount of insolation received by the Earth, which have been shown to greatly influence the climate. At the tropical Mesozoic location of the borehole, this may

have manifested in strength of the seasonal monsoon (Olsen, 1986) the 20-thousand-year precession cycles, in this case, align with low insolation values and therefore wetter climates (Figure 27).

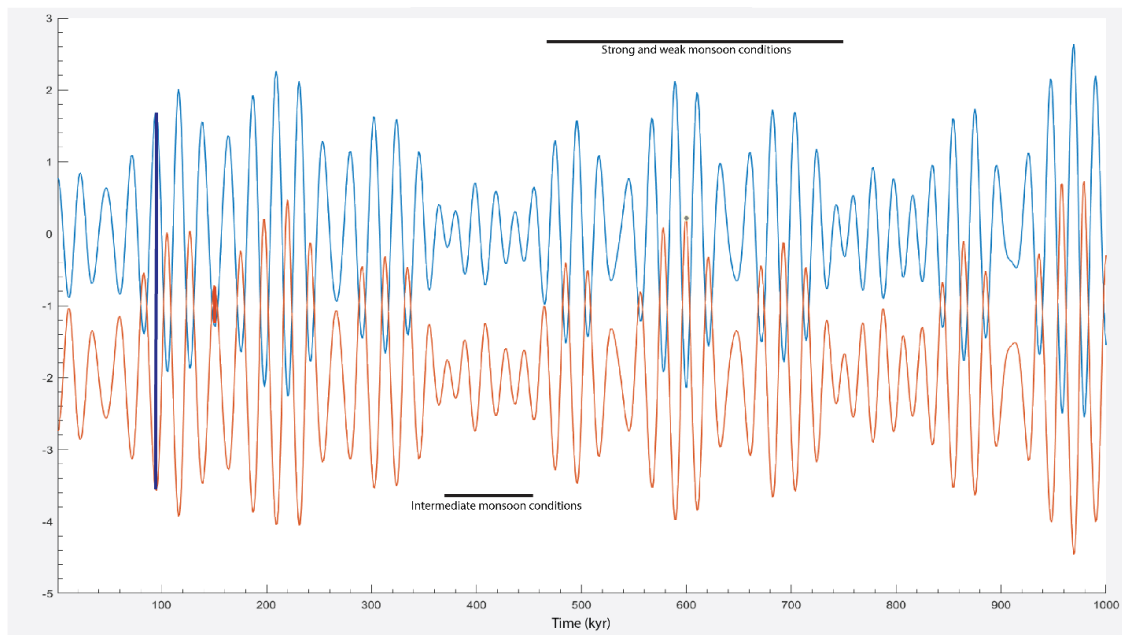


Figure 27. Comparison in relative values of the precession cycle (blue) and the insolation solution (red) using data from Laskar et al., 2004. Vertical blue line shows relationship between precession high and insolation low, indicating a wetter climate. Vertical red line shows relationship between precession low and insolation high, indicating a drier climate. Horizontal black lines overlay a series of precession and insolation cycles and relate the nature of the cycle with monsoon strength.

The lack of a prominent cyclostratigraphy in the lower section of the borehole suggests a more muted insolation response (indicative of drier conditions), as can be seen at 400 kyr (Figure 27). As evidenced by the presence of evaporites and the lack of dark gray deep water shales in the lower portion of the stratigraphy, the drier conditions may have caused the lake to reach evaporative conditions and become a

shallower body of water. The environmental interpretation based on chemical and physical proxies of the borehole further affirms the existence of insolation-related changes that would have happened as a result of the Milankovitch periodicities.

## **5 DISCUSSION**

### *5.1 Correlation of Well Stratigraphy and Regional Stratigraphy*

A similar comparison between records can be made with Olsen's published composite image to place the local stratigraphy into an established basin-wide stratigraphy (Figure 28). Olsen's stratigraphy is derived from artesian well data collected in 1898, two outcropping sites near the Holyoke Dam (42.213°N, -72.602°W) and a core from the Holyoke Dam (Olsen et al, 2003). These sites are approximately 6.5 km south of the MHC borehole. In his stratigraphy, more than 3 colors are used to represent the changes between red, gray, and dark gray, giving the composite the appearance that the shifts between facies are more gradual instead of abrupt. Despite this difference the section matches quite well with the well stratigraphy. Olsen et al.'s stratigraphy spans 656 ft of the record as shown in Figure 28, but it originally spans 250 meters of stratigraphy (Figure 3). The interpreted correlation between the two cores is done based on the assumption that the upper part of Olsen et al.'s composite spans a section of this study's stratigraphy that has been eroded away. Therefore, their lower gray sections correspond to my upper gray sections. The similarities allow for visual correlation of the well stratigraphy with the regional basin stratigraphy as published and interpreted by Olsen et al. The visual

correlation between these two records that is done in this study supports basin wide changes seen in basin stratigraphy rather than localized changes that would be less important, environmentally.

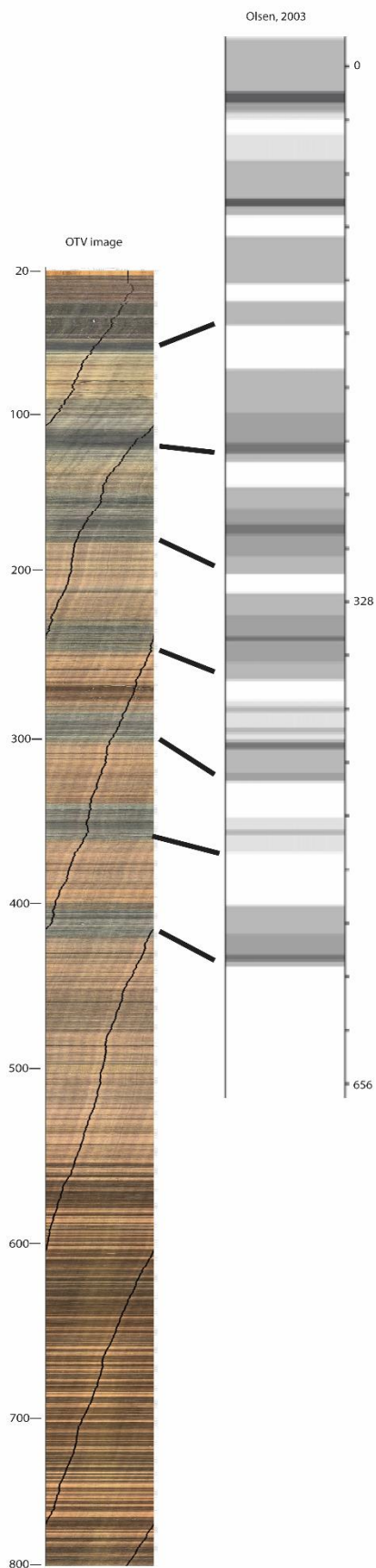


Figure 28. Comparison of borehole (OTV image) stratigraphy and the composite section based on well data at Mount Holyoke and near Holyoke dam (Olsen et al., 2003). Data originally in meters and converted to feet, cropped to fit to page.

Olsen and Kent (1996) have interpreted dark clastic sediments in relation to red clastic sediments present in many rift basins as a sign of changing lake levels. The rift basin lakes of the Northeast are thought to have been less than 100 m deep (Olsen, 1986). In the Newark basin, gray siltstones are described as corresponding to shallow lake conditions, and red mudstones as playa conditions – however, the presence of fossils and microlamination in the gray-black rocks is the main argument for deep water conditions in the Newark basin (Smoot and Olsen, 1994). The Portland formation of the Hartford Basin, however, lacks these microlaminations and fossils (Olsen, 2003, Olsen et al, 2005, Smoot, 1985), suggesting the Hartford basin lake was not as deep as the lake in the Newark Basin – yet, it was deep enough to produce anoxic conditions that formed pyrite in the water column. The Portland formation is also described as having a muted expression of the modulating cycles (Olsen, 2003). This likely refers to the overlying stratigraphy of this study’s borehole, which contains such long intervals of only red mudstone that it cannot be divided into members like the older part of the Portland formation. Muted cyclicity can also be seen in the older part of the 800 ft stratigraphy which lacks dark gray shales. The Portland formation has its “parallel” in the Bontoon formation of the well-studied Newark basin, and the corresponding member there also presents well-developed gray beds in its stratigraphy (Olsen et al., 2005). The independent relationship between the two basins is important, as although each basin is different from the other, the Newark basin has been extensively cored.

### *5.1 Orbital controls on stratigraphy*

The South Hadley Falls member of the Portland formation, whose lower section is shown between 0-400 ft in the borehole, has been described as having the greatest development of grey beds and the greatest amount of evaporitic pseudomorphs compared to anywhere else in the Hartford basin (Olsen et al., 2005). To harbor both of these characteristics, the climate would have had to shift from very wet to very dry. The explanation for this seemingly paradoxical combination of conditions has to do with the g<sub>3</sub>-g<sub>4</sub> eccentricity cycle, where g<sub>3</sub> and g<sub>4</sub> are related to secular frequencies of the precession of the perihelion of Earth and Mars, respectively (Laskar et al., 2004). This long eccentricity cycle has a periodicity of 1.75 million years during the Triassic, and after projecting it from the beginning of the Passaic formation in the Newark basin, the first precessional minimum coincides with the beginning of the South Hadley Falls member (Olsen et al., 2005). Essentially, the interaction between the frequency of the precession of the perihelion of Earth and Mars influences the precession and 100 kyr eccentricity cycles on Earth, which were at a minimum during the time of deposition of the South Hadley Falls member. The deposition of the gray beds and evaporite pseudomorphs could only take place if precession and eccentricity cycles were at a minimum resulting in dryer conditions (Olsen et al., 2005).

## *5.2 Open and closed basin conditions*

Evidence for closed and open basin conditions in the Portland formation is also supported in the literature (Olsen et al., 2005, Olsen, 2003). During open basin conditions, a lake has an outlet through which it is constantly flushed out, forbidding evaporite precipitation in the sediment. During closed basin conditions, however, the basin has no outlet, and water loss occurs through evaporation, which can leave behind evaporite minerals. A lack of evaporite pseudomorphs and a lack of S abundance in the red beds between 0-400 ft suggest intermediate water level conditions, during which the basin is closed but the rate of evaporation is less than the rate of precipitation. The MHC borehole is located relatively close to the eastern edge of the Hartford basin. The proximity to this eastern shoreline may have facilitated this part of the basin in becoming an open/closed system over the years.

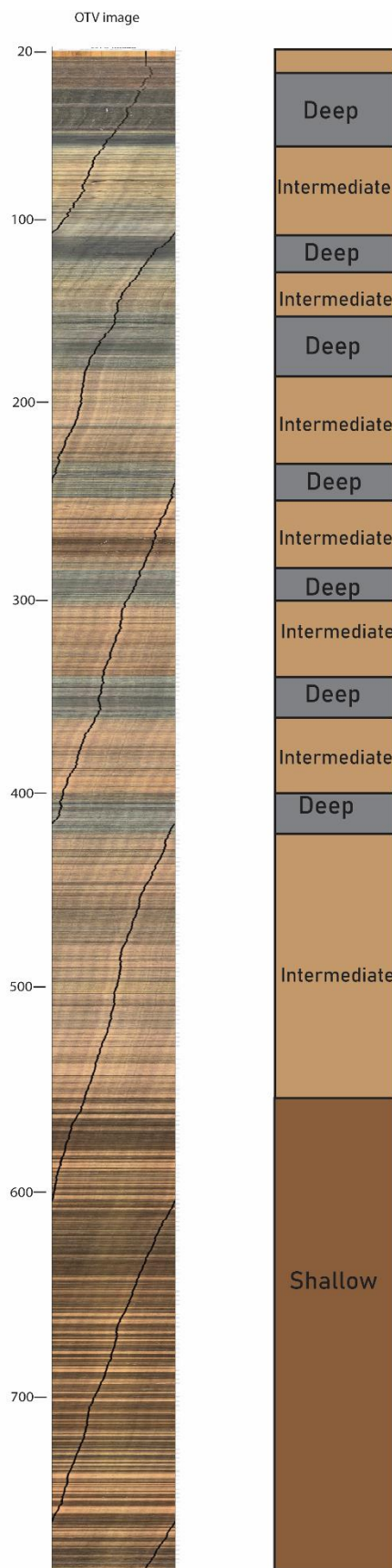


Figure 29. OTV borehole image (left) vs depth interpretation associated with units in the stratigraphy (right).

## **6 CONCLUSION**

The stratigraphy shown in the MHC 800 ft borehole suggests fundamentally changing lacustrine environments over the course of 280 thousand years in the early Jurassic. The record contains significant cyclical activity in the upper 400 feet of the borehole. The resolution (5 ft samples) of the borehole cuttings proxies (XRF, MS, LOI) were sufficient to determine stratigraphic changes for the South Hadley Falls member. The cyclical stratigraphy was present in the color changes of the rocks with depth in the image and cuttings retrieved from the borehole drilling, the MS and LOI proxies gathered from the cuttings, and natural gamma ray data. The borehole's stratigraphy is also confidently related to Milankovitch orbital forcing. The statistical significance of astronomically driven cyclicity was determined using *TimeOpt*, a data-driven method that is reinforced by a linear model that incorporates precession and eccentricity values. *TimeOpt* also output a sedimentation rate for the stratigraphy, suggesting that the borehole contains 283.5 thousand years when considering the entire borehole.

The elemental data gathered by XRF did not by itself reflect cyclicity, but its interpretation was key in the subsequent interpretation of the Jurassic paleoclimate.

Peaks in S in the upper 400 ft were correlated with peaks in Fe, which coupled with macroscopic, euhedral pyrite present in the borehole cuttings, has been interpreted as reducing conditions during deep water, open basin conditions. Uranium peaks in the upper 400 ft and the occurrence of pyrite also supported these deep water phases. Sulfur peaks in the lower half of the record are interpreted as sulfates, which coupled with the occurrence of gypsum present in the borehole cuttings and visible in the borehole images, has been interpreted as the lake having evaporitic conditions in a closed basin. Low S values in other red beds suggest an intermediate environment, where even though the basin was closed, it was not shallow enough for evaporitic conditions. Therefore, this study supports the conclusion that at least three environments of deposition are suggested by the borehole stratigraphy. This interpreted stratigraphy indicates the existence not of a long-lasting rift valley lake in the CRV during the Early Jurassic, but of a lake that frequently changed in response to changing environmental conditions. These changes show periodicities consistent with orbital forcing, demonstrating that long-term climate (with significant changes in the region's hydrologic setting) is determined at least in part by astronomical forcing.

## **7 FUTURE WORK**

Future work should include a closer examination of the elemental chemistry of the cuttings by employing a more refined method of detecting elemental abundances to interpret the elemental properties and correlate them to changing environments accurately and confidently. This could include enhanced sample preparation (powdering each sample) and perhaps whole sample XRF analysis. The chemistry of the Sulfur in particular is very interesting, and more research needs to be conducted regarding Sulfur activity as a geochemical proxy. The analysis of other elements that are also redox sensitive, like Manganese and Iron in different oxidation states and relative to each other (ratios), should also be investigated at a higher resolution. Preliminary investigation for this study suggests that changes in these elements are significant enough to warrant more chemistry work to be done on this specific borehole.

The lower section of this stratigraphy, which belongs to the upper section of the Park River member, reveals a variable red stratigraphy that includes rhythmic, primary gypsum deposits (Figure 10). A closer look at this section reveals that the gypsum spacing is relatively consistent (1 gypsum band/4.5 inches). Considering the

consistency of the short cyclicity in this section of the borehole, a closer look at this section is warranted. Possible next steps include oxygen isotope analysis to better understand the evaporitic conditions that the lower 500 ft of the borehole suggest, and to further establish that the gypsum presence in the borehole is primary. Devoting more time to analysis of this section would be the first steps in better understanding the environment of deposition where Milankovitch forcing is not visually apparent.

The prospect of more interdisciplinary research between geology, astronomy, chemistry, and physics to accurately determine Milankovitch astronomical forcing and other long modulating orbital cycles affecting the stratigraphy of the Northeast, should also be pursued. Sophisticated and appropriate models for correlating stratigraphic proxies with astronomical forcing, such as those found in the *Acycle* program (including *TimeOpt*) are highly worthy of future research in this area. Therefore, attention to the development of models and efforts geared toward the accurate determination of cyclicity in other paleo-proxies should be invested in as well.

The stratigraphy of the South Hadley Falls member of the Portland Formation in the Hartford basin appears to contain a similar record to the stratigraphy more thoroughly analyzed and interpreted in the Newark basin. A coring project of the Hartford Basin (much like the Newark Coring project (Goldberg et al., 1994; Olsen and Kent, 1990)) would provide a greater understanding of the context of this study by having high resolution stratigraphy of the other formations of the Hartford basin.

## **8 REFERENCES**

- Baker, G.S., 1994. An examination of Triassic cyclostratigraphy in the Newark Basin from shallow seismic profiles and geophysical logs. Lehigh University. Masters Theses.
- Blackburn, T.J., Olsen, P.E., Bowring, S.A., McLean, N.M., Kent, D.V., Puffer, J., McHone, G., Rasbury, E.T., Et-Touhami, M. 2013. Zircon U-Pb geochronology links the end-Triassic extinction with the Central Atlantic Magmatic Province. *Science* 340, 941–945.
- Bruker Corporation. NA. S1 TITAN/TRACER 5' User Manual. #030.0112.01.0
- Chorowicz, J. 2005. The East African rift system. *Journal of African Earth Sciences* 43:379-410.
- Chou, C.L., 2012. Sulfur in coals: A review of geochemistry and origins. *International Journal of Coal Geology* 100: 1-13.
- Cohen, A.S. 2003. *Paleolimnology: The History and Evolution of Lake Systems*. Oxford University Press, Oxford, New York.
- Crowley, T.J., Kim, K.Y., Mengel, J.G., Short, D.A., 1992, Modeling 100,000-Year Climate Fluctuations in Pre-Pleistocene Time Series. *Science* v. 255, p, 705-707.
- Ding, X., Li, D., Zheng, L., Bao, H., Chen, H-F., Kao, S-J., 2016. Sulfur Geochemistry of a Lacustrine Record from Taiwan Reveals Enhanced Marine Aerosol Input during the Early Holocene. *Scientific Reports*, 12;6:38989.
- Emerson, B.K., 1898 *Geology of old Hampshire County, Massachusetts : comprising Franklin, Hampshire, and Hampden counties*. U.S Geological Survey, Monograph 29, 1-790.
- Gale, S.J., Hoare, P.G., 1991. *Quaternary Sediments: Petrographic Methods for the Study of Unlithified Rocks - Chapter 4.7: The magnetic susceptibility of regolith materials (201-230)*. Bellhaven Press, London, UK.

- Goldberg, D.S., Reynolds, D.J., Williams, C.F., White, W.K., Olsen, P.E., Kent, D.V., 1994. Well logging results from the Newark Rift Basin Coring Project. *Scientific Drilling*, 4: 267-279.
- Hager-Reichter Geosciences, Inc., 2020. BOREHOLE GEOPHYSICAL LOGGING – DATA REPORT GEOTHERMAL WELL MOUNT HOLYOKE COLLEGE SOUTH HADLEY, MASSACHUSETTS. Prepared for: Skillings & Sons, Inc. South Hadley, MA.
- Hilton, J. 1986. Normalized magnetic parameters and their applicability to paleomagnetism and environmental magnetism. *Geology*, 14(10): 887-889.
- Hitchcock, E. 1858. *Ichnology of New England: A Report on the Sandstone of the Connecticut Valley Especially Its Fossil Footmarks, Made to the Government of the Commonwealth of Massachusetts*. William White, Boston, Massachusetts.
- Kenna, C.T., Nitsche, F.O., Herron, M.M., Mailloux, B.J., Peteet, D., Sritrairat, S., Sands, E., Baumgarten, J. 2011. Evaluation and calibration of a Field Portable X-Ray Fluorescence spectrometer for quantitative analysis of siliciclastic soils and sediments. *Journal of Analytical Atomic Spectrometry*, 26:395-405.
- Kent, D. V., and Olsen P. E. 2008. Early Jurassic magnetostratigraphy and paleolatitudes from the Hartford continental rift basin (eastern North America): Testing for polarity bias and abrupt polar wander in association with the central Atlantic magmatic province, *J. Geophys. Res.*, 113.
- Kent, D.V., Olsen, P.E., 1990. Continental Coring of the Newark Rift. *EOS, Trans. of the American Geophysical Union*. 71: 385, 394.
- Kent, D.V., Tauxe, L. 2005. Corrected Late Triassic latitudes for continents adjacent to the North Atlantic. *Science* 307, 240-244.
- Kutzbach, J.E., Street-Perrott, F.A., 1985. Milankovitch forcing of fluctuations in the level of tropical lakes from 18 to 0 kyr. *Nature*, 317, 130-134.
- Laskar, J. 2020. Chapter 4 - Astrochronology, in: Ogg, J.G., Schmitz, M.D., Ogg, G.M. (Eds.), *Geologic Time Scale 2020*. Elsevier, Amsterdam, pp. 139-158.

Laskar, J., Robutel, P., Joutel, F., Gastineau, M., Correia, A.C.M., Levrard, B., 2004. A long-term numerical solution for the insolation quantities of the Earth. *Astronomy & Astrophysics*, 428, 261-285.

Li, M., Hinnov, L.A., and Kump, L.R. 2019. Acycle: Time-series analysis software for paleoclimate projects and education, *Computers & Geosciences*, 127: 12-22.

Little, R.D., 2003. *Dinosaurs, Dunes, and Drifting Continents: The Geology of the Connecticut River Valley 3rd Edition*. Earth View LLC.

Meyers, S. R. (2015), The evaluation of eccentricity-related amplitude modulation and bundling in paleoclimate data: An inverse approach for astrochronologic testing and time scale optimization, *Paleoceanography*, 30, 1625–1640

Mitchinson-Field, L. 2016. *Assessing Stratigraphy Under the Mount Holyoke Campus*. Mount Holyoke College.

Olsen, P. E. and Kent, D. V., 1996, Milankovitch climate forcing in the tropics of Pangea during the Late Triassic. *Palaeogeography, Palaeoclimatology, and Palaeoecology*, v. 122, p. 1-26

Olsen, P.E., Kent, D.V., 1999. Long-period Milankovitch cycles from the Late Triassic and Early Jurassic of eastern North America and their implications for the calibration of the Early Mesozoic time-scale and the long-term behaviour of the planets. *The Royal Society*, 357, 1761 - 1786.

Olsen, P. E., 1986, A 40-million-year lake record of early Mesozoic climatic forcing. *Science*, v. 234, p. 842-848.

Olsen, P.E., 1997. Stratigraphic record of the early Mesozoic breakup of Pangea in the Laurasia-Gondwana rift system. *Annual Reviews of Earth and Planetary Science* 25, 337-401.

Olsen, P.E., 2017, *Origins of Dinosaur Dominance in the Connecticut Valley Rift Basin*. A Field Trip Sponsored by the Keck Foundation & Hosted by Wesleyan University, Keck Geological Consortium, p. 2-46

Olsen, P.E., Whiteside, J.H., and Huber, P., 2003, Causes and consequences of the Triassic-Jurassic mass extinction as seen from the Hartford basin. in Brady, J. B. and

Cheney, J.T. (eds.) Guidebook for Field Trips in the Five College Region, 95th New England Intercollegiate Geological Conference, Department of Geology, Smith College, Northampton, Massachusetts, p. B5-1 - B5-41.

Olsen, P.E., Whiteside, J.H., LeTourneau, P.M., and Huber, P., 2005, Jurassic cyclostratigraphy and paleontology of the Hartford basin. In B.J. Skinner and A.R. Philpotts (eds.), 97th New England Intercollegiate Geological Conference, Department of Geology and Geophysics, Yale University, New Haven, Connecticut, p. A4-1 - A4-51

Pasternack, G. NA. Loss on Ignition Protocol. Recovered from:  
<http://pasternack.ucdavis.edu/research/methods/loss-ignition-protocol/>

Robertson, S. 2011. Direct Estimation of Organic Matter by Loss on Ignition: Methods. SFU Soil Science Lab.

Russell, J.M.; Barker, P.; Cohen, A.; Ivory, S.; Kimirei, I.; Lane, C.; Leng, M.; Maganza, N.; McGlue, M.; Msaky, E.; Noren, A.; Park Boush, L.; Salzburger, W.; Scholz, C.; Teidemann, R.; Nuru, S., 2020. ICDP workshop on the Lake Tanganyika Scientific Drilling Project: a late Miocene–present record of climate, rifting, and ecosystem evolution from the world’s oldest tropical lake. *Scientific Drilling*, v. 27, p. 53-60.

Sha, J., Olsen, P.E., Xu, D., Yao, X., Pan, Y., Wang, Y., Zhang, X., Vajda, V., 2015. Early Mesozoic, high-latitude continental Triassic–Jurassic climate in high-latitude Asia was dominated by obliquity-paced variations (Junggar Basin, Urumqi, China). *Proceedings of the National Academy of Sciences* 112, 3624-3629.

Szecsody, J.E., Cantrell, K.J., Krupka, K.M., Resch, C.T., Williams, .M.D., Fruchter, J.S., 1998. Uranium Mobility During In Situ Redox Manipulation of the 100 Areas of the Hanford Site. Prepared for the US Department of Energy, available from: National Technical Information Service, US Department of Commerce.

Serfes, M., Herman, G., Spayd, S., Reinfelder, J., 2010. Sources, mobilization and transport of arsenic in groundwater in the Passaic and Lockatong Formations of the Newark Basin. In "Contributions to the Geology and Hydrogeology of the Newark Basin"., NJ Geological Survey Bulletin 77.

Smoot, J. P. and Olsen, P. E., 1994, Climatic cycles as sedimentary controls of rift basin lacustrine deposits in the early Mesozoic Newark basin based on continuous core. in Lomando, A. J. and Harris, M., Lacustrine Depositional Systems, SEPM Core Workshop Notes, v. 19, p. 201-237

Smoot, J. 1985. The closed-basin hypothesis and its use in facies analysis of the Newark Supergroup in "Proceedings of the Second U.S. Geological Survey Workshop on the Early Mesozoic Basins of the Eastern United States" U.S. Geological Survey Circular 946.

Stanley, S.M., Luczaj, J.A., 2014. Earth System History - Chapter 16: The Early Mesozoic Era. W.H Freeman and Company, 389-420.

Stüeken, E.E., Martinez, E., Love, G., Olsen, P.E., Bates, S., Lyones, T.W., 2019. Effects of pH on redox proxies in a Jurassic rift lake: Implications for interpreting environmental records in deep time. *Geochimica et Cosmochimica Acta*, 252, 240 - 267.

Turner-Peterson, C. E., Olsen, P. E., Nuccio, V. F., 1985, Modes of Uranium occurrence in the Newark Basin, New Jersey and Pennsylvania: U.S. Geological Survey Circular 946, p. 120- 124.

Whiteside, J.H., Grogan, D.S., Olsen, P.E., Kent, D.V. 2011. Climatically driven biogeographic provinces of Late Triassic tropical Pangea. *Proceedings of the National Academy of Sciences* 108, 8972–8977.

Van Houten, F., 1962. Cyclic Sedimentation and the Origin of Analcime-Rich Upper Triassic Lockatong Formation, West-Central New Jersey and Adjacent Pennsylvania. *American Journal of Science*, v. 260, p. 561-576.

Yang, H., Huang, Y., Ma, C., Zhang, Z., Wang, C., 2020. Recognition of Milankovitch cycles in XRF core-scanning records of the Late Cretaceous Nenjiang Formation from the Songliao Basin (northeastern China) and their paleoclimate implications. *Journal of Asian Earth Sciences*, 194:104183.

**9 SUPPLEMENTARY MATERIALS**

Table 1. MS Raw data.

DEPTH	MS (SI)
0	71
5	75
10	61
15	35
20	58
25	71
30	84
35	26
40	29
45	19
50	6
55	15
60	10
65	8
70	35
75	32
80	34
85	46
90	69
95	14
100	22
105	14
110	14
115	17
120	23

125	20
130	32
135	57
140	84
145	66
150	44
155	18
160	12
165	12
170	11
175	12
180	60
185	72
190	71
195	35
200	52
205	54
210	38
215	42
220	55
225	61
230	17
235	16
240	11
245	35
250	39
255	41
260	37
265	29
270	34
275	28

280	45
285	-
290	13
295	14
300	14
305	30
310	40
315	42
320	46
325	37
330	35
335	30
340	17
345	16
350	8
355	9
360	22
365	58
370	41
375	33
380	40
385	29
390	40
395	30
400	38
405	14
410	11
415	14
420	29
425	34
430	13

435	28
440	37
445	41
450	31
455	53
460	42
465	27
470	35
475	41
480	26
485	32
490	28
495	27
500	15
505	34
510	33
515	32
520	28
525	26
530	36
535	23
540	26
545	17
550	16
555	24
560	18
565	27
570	18
575	18
580	14
585	12

590	13
595	13
600	12
605	13
610	11
615	14
620	23
625	15
630	23
635	35
640	12
645	12
650	9
655	10
660	14
665	18
670	13
675	11
680	10
685	9
690	11
695	12
700	12
705	13
710	10
715	9
720	9
725	11
730	13
735	13
740	12

745	11
750	14
755	6
760	8
765	8
770	10
775	9
780	13
785	11
790	13
795	32
800	16

Table 2. LOI Raw data.

Depth (ft)	LOI (%)
0	0.4652
5	0.7052
10	0.6432
15	0.6565
20	0.5209
25	0.7932
30	2.082
35	2.614
40	2.300
45	4.230
50	3.915
55	3.362
60	4.342
65	1.373
70	2.895
75	1.108
80	1.607
85	0.9361
90	1.622
95	2.386
100	2.853
105	3.177
110	3.586
115	5.663
120	4.856
125	1.249
130	0.6057
135	0.6632
140	0.7771

145	0.6747
150	1.090
155	1.083
160	1.297
165	1.473
170	1.485
175	1.213
180	1.410
185	0.8629
190	0.9374
195	0.3012
200	0.9286
205	0.6083
210	1.092
215	0.8246
220	1.098
225	0.8393
230	1.082
235	1.004
240	1.074
245	0.5789
250	0.8782
255	0.7420
260	0.5798
265	0.6316
270	0.6087
275	0.6832
280	1.068
285	N/A
290	1.250
295	1.212

300	1.268
305	0.7356
310	0.5667
315	0.8441
320	0.7221
325	1.141
330	0.8675
335	1.223
340	2.345
345	3.738
350	1.510
355	2.034
360	0.9116
365	0.6280
370	0.4977
375	0.4826
380	0.4274
385	0.7685
390	0.5918
395	0.8255
400	1.126
405	1.450
410	1.075
415	1.180
420	1.108
425	0.6989
430	0.4857
435	0.7546
440	0.9398
445	0.9108
450	1.109

455	0.8706
460	0.8896
465	1.189
470	1.252
475	1.084
480	0.5850
485	0.5299
490	0.3964
495	0.6208
500	0.2333
505	0.5725
510	0.7490
515	0.6760
520	0.6351
525	0.5530
530	0.5739
535	0.3573
540	0.8040
545	0.8399
550	0.8633
555	1.350
560	1.262
565	1.384
570	1.116
575	1.141
580	1.138
585	1.162
590	1.077
595	1.170
600	0.6747
605	0.7804

610	0.9194
615	0.8356
620	1.323
625	1.472
630	1.523
635	1.594
640	1.179
645	0.8833
650	0.8999
655	0.8133
660	1.288
665	2.613
670	1.171
675	1.553
680	1.046
685	1.669
690	1.145
695	1.140
700	1.347
705	1.967
710	1.129
715	0.7665
720	0.7581
725	0.9677
730	1.145
735	1.730
740	1.706
745	1.142
750	1.011
755	0.7556
760	0.6034

765	0.6891
770	0.6547
775	0.7553
780	1.082
785	1.073
790	1.916
795	2.008
800	3.454

Table 3. XRF Raw data.

Depth	Sulfur	Iron	Uranium
5	0.0302	2.575	NA
10	NA	3.112	NA
15	0.0277	3.262	NA
20	0.0178	3.217	NA
25	0.1375	5.516	NA
30	0.0357	3.717	NA
35	0.6275	3.893	0.0031
40	0.156	3.987	NA
45	0.2285	4.149	NA
50	0.2028	3.820	NA
55	0.8528	4.370	NA
60	0.2591	1.940	0.0024
65	2.8233	4.457	NA
70	0.0495	3.780	NA
75	0.0462	3.081	NA
80	0.0184	3.475	NA
85	0.0859	2.331	NA
90	0.4018	2.892	NA
95	2.9635	5.157	NA
100	2.59	5.527	NA
105	0.15	3.568	NA
110	0.2197	3.520	0.0018
115	0.3507	3.387	0.002
120	0.5295	2.933	NA
125	3.3601	5.831	NA
130	0.0567	2.435	NA
135	0.2464	2.614	NA
140	0.0879	3.196	NA
145	0.0268	3.278	NA

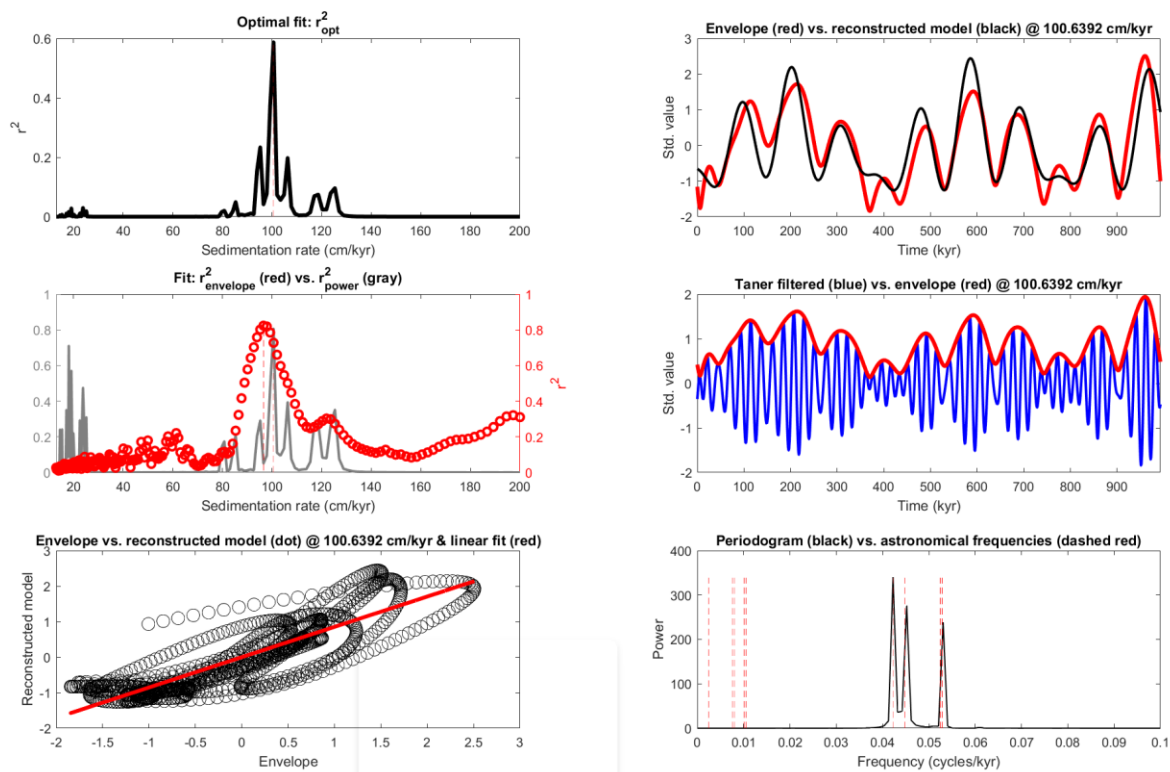
150	0.0331	3.553	NA
155	0.03	3.695	NA
160	0.7074	3.301	NA
165	0.346	2.845	0.0034
170	0.6049	2.675	0.0049
175	2.8325	5.613	NA
180	0.0511	3.353	NA
185	0.0298	3.112	NA
190	0.0173	3.300	NA
195	0.0394	1.300	NA
200	0.0359	2.304	NA
205	NA	3.188	NA
210	NA	2.817	NA
215	NA	4.069	NA
220	NA	2.279	NA
225	0.0268	2.744	NA
230	0.1302	4.455	0.0017
235	0.3678	3.402	0.0028
240	0.1165	4.984	NA
245	0.025	3.407	NA
250	0.1706	4.166	NA
255	0.0227	3.928	NA
260	0.0217	3.389	NA
265	NA	3.223	NA
270	0.1088	5.619	NA
275	0.022	2.171	NA
280	0.0203	4.990	NA
290	0.4423	2.452	0.0048
295	0.2245	2.825	NA
300	0.0376	3.862	NA
305	0.0238	2.678	NA

310	0.053	1.820	NA
315	NA	3.267	NA
320	0.0251	3.576	NA
325	NA	3.030	NA
330	NA	6.199	NA
335	NA	5.152	NA
340	0.0409	2.429	NA
345	0.0478	4.547	NA
350	0.153	5.567	NA
355	0.3564	3.656	0.002
360	0.3944	2.855	0.0034
365	2.2508	4.093	NA
370	0.1222	3.337	NA
375	0.0157	3.545	NA
380	0.0174	2.681	NA
385	NA	2.431	NA
390	0.0216	3.543	NA
395	NA	4.253	NA
400	0.0562	3.862	NA
405	0.0317	3.417	NA
410	0.045	3.556	NA
415	0.3453	3.528	0.0187
420	1.8536	5.670	NA
425	0.3428	2.844	0.0039
430	0.2027	2.260	NA
435	0.0179	3.779	NA
440	0.0295	2.273	NA
445	NA	3.769	NA
450	0.0248	2.352	NA
455	0.0386	3.819	NA
460	0.0324	3.525	NA

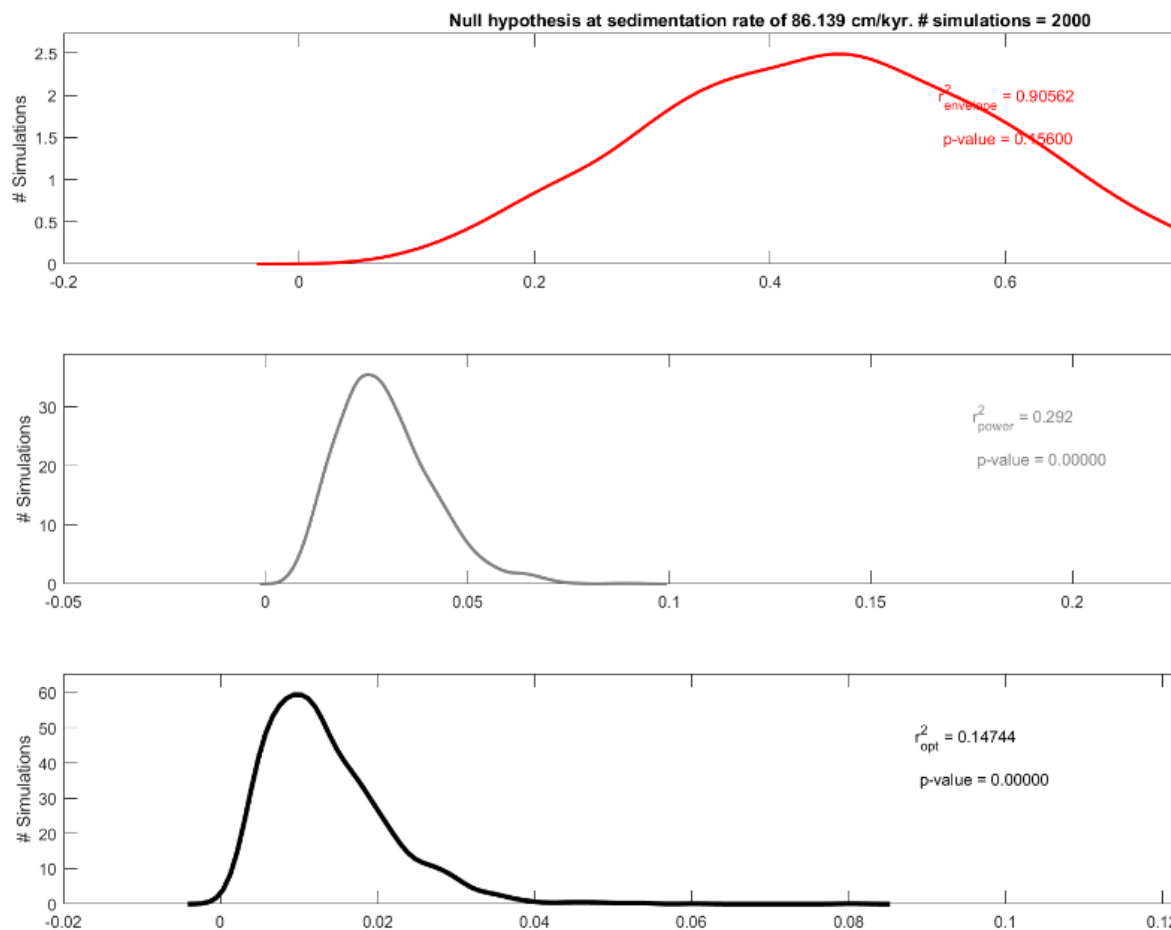
465	0.0437	3.709	NA
470	0.0549	3.552	NA
475	0.034	2.932	NA
480	0.0342	3.960	NA
485	NA	4.255	NA
490	0.0398	4.425	NA
495	0.0274	3.018	NA
500	0.0405	1.950	NA
505	0.0379	3.594	NA
510	0.036	1.322	NA
510	0.0238	2.809	NA
515	0.0229	3.484	NA
520	0.0259	4.215	NA
525	0.0435	3.884	NA
530	0.0221	2.653	NA
535	0.034	4.167	NA
540	0.0944	2.482	NA
545	0.0565	1.277	NA
550	0.0212	2.893	NA
555	0.0225	3.793	NA
560	0.0434	3.584	NA
565	0.0839	3.421	NA
570	0.0315	3.850	NA
575	0.0549	4.247	0.0022
580	0.0446	4.053	NA
585	0.2482	3.719	NA
590	0.2814	3.918	NA
595	0.3956	4.932	NA
600	0.0521	3.060	NA
605	1.0804	2.036	NA
610	0.1108	4.582	NA

615	0.1133	3.077	NA
620	3.8455	3.580	NA
625	0.1168	3.584	NA
630	3.024	4.246	NA
635	0.0978	4.202	NA
640	4.9633	3.068	NA
645	0.3999	3.937	NA
650	0.4489	2.776	NA
655	0.1607	2.923	NA
660	0.3702	4.300	NA
665	0.0999	3.023	NA
670	0.5192	3.350	NA
675	2.117	2.680	NA
680	0.3987	3.791	NA
685	0.5864	4.079	NA
690	0.079	4.029	NA
695	2.6767	3.462	NA
700	5.1136	5.694	NA
705	0.6194	4.629	NA
715	0.5572	3.001	NA
720	0.3649	2.433	NA
725	0.3494	2.607	NA
725	0.0899	3.416	NA
730	2.7036	4.211	NA
735	0.0693	3.731	NA
740	0.8192	4.050	NA
745	0.1034	2.502	NA
750	0.057	3.539	NA
755	0.0998	2.592	NA
760	0.1955	4.025	NA
765	0.0241	3.864	0.0022

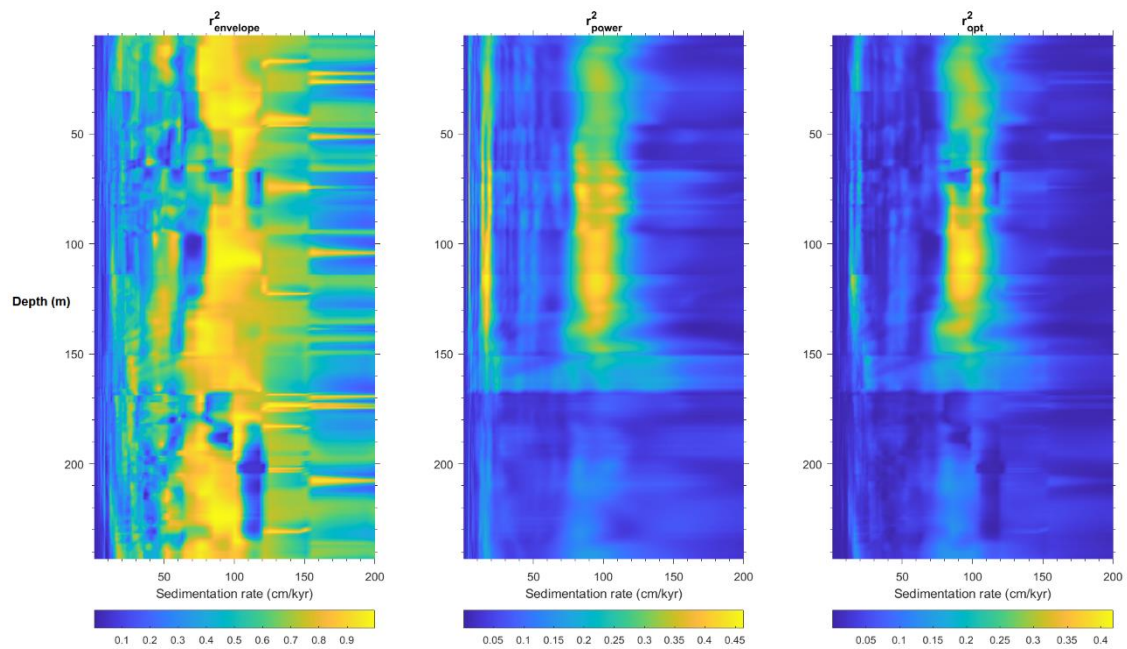
770	0.5497	2.599	NA
775	2.1361	5.252	NA
780	0.6086	2.442	NA
785	0.0388	4.386	NA
790	0.0626	3.878	NA
795	0.0526	5.095	NA
800	0.4801	3.664	NA



Supplementary Figure 1. *TimeOpt* output for the Laskar et al 2004 precession solution. Note the  $r^2_{opt} = 0.6$ , and the fit of the data with the model.



Supplementary Figure 2. Monte Carlo simulations done on the natural gamma ray log stratigraphy's optimal sedimentation rates and the TimeOpt models.  $r^2_{\text{opt}}$  p-value = 0.00000



Supplementary Figure 3. *eTimeOpt* output for the natural gamma ray log. Correlation is shown in color legend for  $r^2_{\text{envelope}}$ ,  $r^2_{\text{power}}$ , and  $r^2_{\text{opt}}$ . Highest correlation in  $r^2_{\text{opt}}$  happens at  $\sim 90$ cm/kyr.